

Library Copy
A. A212160 R.O.1

~~CONFIDENTIAL~~

Copy 42
RM SL56A13

~~UNAVAILABLE~~
C.1
NACA

RESEARCH MEMORANDUM

for the

Bureau of Aeronautics, Department of the Navy

LIFT, DRAG, STATIC STABILITY, AND BUFFET BOUNDARIES

OF A MODEL OF THE McDONNELL F3H-1N AIRPLANE

AT MACH NUMBERS FROM 0.40 TO 1.27

TED NO. NACA DE 351

By Norman L. Crabill

Langley Aeronautical Laboratory
Langley Field, Va.

CLASSIFIED DOCUMENT

This document contains classified information affecting the National Defense of the United States within the meaning of the Espionage Act, USC 18793 and 794. Its transmission or the revelation of its contents in any manner to an unauthorized person is prohibited by law.

**NATIONAL ADVISORY COMMITTEE
FOR AERONAUTICS**
WASHINGTON

JAN 31 1956
~~CONFIDENTIAL~~

UNAVAILABLE

UNCLASSIFIED

To:

By authority of

Date



NATIONAL ADVISORY COMMITTEE FOR AERONAUTICS

RESEARCH MEMORANDUM

for the

Bureau of Aeronautics, Department of the Navy

LIFT, DRAG, STATIC STABILITY, AND BUFFET BOUNDARIES

OF A MODEL OF THE McDONNELL F3H-1N AIRPLANE

AT MACH NUMBERS FROM 0.40 TO 1.27

TED NO. NACA DE 351

By Norman L. Crabill

SUMMARY

The National Advisory Committee for Aeronautics has conducted a flight test of a model approximating the McDonnell F3H-1N airplane configuration to determine its pitch-up and buffet boundaries, as well as the usual longitudinal stability derivatives obtainable from the pulsed-tail technique. The test was conducted by the freely flying rocket-boosted model technique developed at the Langley Laboratory; results were obtained at Mach numbers from 0.40 to 1.27 at corresponding Reynolds numbers of 2.6×10^6 and 9.0×10^6 . The phenomena of pitch-up, buffet, and maximum lift were encountered at Mach numbers between 0.42 and 0.85. The lift-curve slope and wing-root bending-moment slope increased with increasing angle of attack, whereas the static stability decreased with angle of attack at subsonic speeds and increased at transonic speeds. There was little change in trim at low lift at transonic speeds.

INTRODUCTION

At the request of the Bureau of Aeronautics, Department of the Navy, the National Advisory Committee for Aeronautics tested a 1/10-scale model of the McDonnell XF3H-1 DEMON airplane in free flight with the purpose of determining the effect of the operation of extensible rocket racks on its aerodynamic characteristics. Data from this test are presented in

~~CONFIDENTIAL~~

reference 1. In the course of this test a high angle of attack, longitudinal instability, and associated severe buffeting were discovered to exist at subsonic Mach numbers. In order to study these and other problems on one of the production configurations of this airplane, the NACA has since tested a model approximating the F3H-1N configuration by the free-flight pulsed-tail technique. The results of this test are presented in this report and compared with estimates of the aerodynamic characteristics of this same configuration. These estimates were based on wind-tunnel tests of the XF3H-1 and the F3H-1N configurations.

The model was supplied by the McDonnell Aircraft Corporation, and the test was made at the Langley Pilotless Aircraft Research Station at Wallops Island, Va.

DESCRIPTION OF MODEL AND INSTRUMENTATION

Model

The model used in this test was originally built as one of four 1/10-scale models of the McDonnell XF3H-1 airplane, and was identical to the models described in references 1 and 2. However, the McDonnell Aircraft Corporation subsequently modified this model by removing the existing extensible rocket rack mechanism, incorporating an F3H-1N wing, relocating the XF3H-1 horizontal tail to the F3H-1N position, and enlarging the underside of the tail boom slightly to accommodate the servo-piston and push rod necessary to pulse the entire horizontal stabilizer. The principal difference between this resulting configuration and the actual F3H-1N configuration is that the F3H-1N configuration has a fatter fuselage and somewhat larger horizontal tail. The electro-hydraulic system was designed to pulse this surface in a square wave motion between stops of $+1^\circ$ (dwell time 1.0 second) and -3° (dwell time 0.5 second) measured relative to the fuselage reference line.

The three-view drawing in figure 1(a), and table I give the important dimensions and mass properties; a general view of the model is furnished in figure 1(b). The F3H-1N plan form was derived from the XF3H-1 plan form by adding a constant-chord (0.91 inch, model scale) leading-edge extension to the XF3H-1 wing and by some slight alteration of the tip fairing, figure 1(c). Since the absolute maximum thickness was held constant, the relative thickness is proportionately reduced. The various natural frequencies and modes of vibration of the model shown in figure 1(d) were determined by feel, hearing, and sight while oscillating it at various frequencies with an electromagnetic shaker. The telemeter traces of the accelerometers and the wing bending - strain gage obtained when the model was shaken and when the principal components of the model

were struck were also examined to obtain the resonant frequencies which are noted in figure 1(d).

Instrumentation

The model was instrumented to transmit continuous records of ten quantities: (1) fuselage angle of attack, (2) normal acceleration at the center of gravity, (3) normal acceleration at the pilot's seat, (4) longitudinal acceleration at the center of gravity, (5) transverse acceleration near the center of gravity, (6) stabilizer deflection relative to the fuselage reference line, (7) pitot total head, (8) absolute static pressure behind the angle-of-attack indicator base, (9) wing bending moment, and (10) an absolute static pressure on the upper surface of the wing. Measurements (8) and (10) were judged to be unreliable and were not used. The bending-moment strain-gage location and the pressure orifice location are shown in figure 1(a); the photograph (fig. 1(e)) shows the installation of these instruments in the right wing panel. It was anticipated that these instruments would be of value in studying any buffet phenomena encountered.

Shortly before the test, a rawinsonde was released to obtain atmospheric temperature, pressure, and wind information from sea level to 9,000 feet. During the test, measurements of model velocity and position in space were made from the CW Doppler velocimeter and the NACA modified SCR 584 tracking radar, respectively.

TESTS AND METHODS OF ANALYSIS

The model was tested by the free-flight model technique described in reference 3. The axes systems used herein are shown in figure 2. As the model decelerated from $M = 1.27$ to $M = 0.40$, the results were obtained as time histories and after suitable corrections were applied to the raw data, the quantities M , δ , α_f , C_L , C_D , C_m , C_{BM} , and C_Y were obtained. Time histories of most of these quantities are presented in figures 3(a) and 3(b). The analysis then consisted of making suitable cross plots and inspecting the transients for trim and buffet data. No damping derivatives were determined, since the system proved to be non-linear. The dynamic pressure and Reynolds number of the test are given in figure 4(a) as functions of Mach number, whereas wind velocity and temperature are given as functions of altitude in figure 4(b). From the vertical distribution of temperature and wind velocity, it can be seen that the initial part of the flight took place in unstable air. This may have excited both the model short-period stability oscillation and some structural modes. This latter possibility is discussed in the section entitled "Buffet Boundaries."

RESULTS AND DISCUSSION

General

Inspection of the time histories (fig. 3) indicates that the region of high-angle-of-attack instability sought for was encountered. The longitudinal instability first occurred at $T = 7.5$ seconds and $M = 0.90$ (fig. 3(a)). In the resulting pitch up, a speed slow down of about $\Delta M = 0.12$ was experienced. Subsequent pitch-ups, starting at about $M = 0.70, 0.54$, and 0.46 did not suffer such extreme slow downs, due to the smaller dynamic pressure at the higher altitudes and lower Mach numbers. The model flew a total of 54 seconds and continued to pitch up whenever the stabilizer moved to the trailing-edge-up position; because of the high drag in this condition, the model never exceeded $M = 0.48$ on the descending portion of the flight.

At transonic speeds ($T = 3.2$ to 7.3 seconds) the longitudinal transients were positively damped, although the low lift oscillations ($T \approx 4.5$ and $T \approx 6.5$ seconds) were irregular in character, apparently because of some coupling with the lateral mode or because of the atmospheric turbulence mentioned before.

Trim

The angle of attack of the fuselage reference line and lift coefficient at static trim shown in figures 5(a) and (b) were determined both from their respective time histories and from cross plots of pitching-moment coefficient and angle of attack. The stabilizer deflections necessary to produce these trim levels are given in figure 5(c). Corresponding trim values derived from wind-tunnel data (ref. 4) are in fair agreement at low lift but the variation of trim with Mach number is different.

Lift

The basic lift data consist of cross plots of C_L and α_f , (figs. 6(a) and (b)). Inspection of these plots indicates that the slope increases slightly with increasing angle of attack up to the high-lift break at subsonic speeds, and up to the test limit at transonic speeds. While the actual increase in slope may well be continuous, it seems best to fit two straight lines to the data, giving a low slope at low lift and a somewhat higher slope at moderate lift. These slopes and the angle of attack ranges over which they apply are given in figures 7(a) and (b). The wind-tunnel data of reference 4 indicate either a decreasing lift-curve slope

with increasing angle of attack or a constant slope; the low-lift slope from this source is substantially the same as the moderate-lift slope obtained in the present test (fig. 7(a)). Corrections for upwash at the angle-of-attack indicator and for wing flexibility have not been applied to the present data, but it is estimated that upwash would increase $C_{L\alpha}$ by only 3 percent at $M = 0.40$. No corrections have been applied for wing flexibility, but it was felt that they would be small.

The shapes of the lift curves, figure 6(a) indicate that the model effectively reached $C_{L_{max}}$ several times between $M = 0.42$ and 0.85 . These $C_{L_{max}}$ data are plotted in figure 7(c) and indicate that $C_{L_{max}}$ decreases with increasing Mach number. From $M = 0.6$ to 0.85 , the data show that the maximum-lift coefficient depends significantly on the sign of $d\alpha_F/dt$.

The lift intercept $C_{L_{\alpha_F=0}}$ obtained in this test for $\delta_S = +1^\circ$ is given also in figure 7(c), and is in good agreement with the data from reference 4. The value of $C_{L_S} = 0.0070$ obtainable at $M = 1.15$ from this test (fig. 7(c)) is in good agreement with the data of reference 4, which gives $C_{L_S} = 0.00724$ at $M = 1.15$.

Drag

All drag coefficients in this report include base drag and, since the engine inlet was completely blocked, also include an additive drag due to spillage. (See refs. 1 and 5 for these data.) Furthermore, since the fuselage employed on the actual F3H-1N configuration is somewhat fatter, there may be an important difference in the minimum drag. The basic data are presented as cross plots of C_D and C_L (figs. 8(a) and (b)) from which $C_{D_{min}}$ and C_L for $C_{D_{min}}$ were determined. The induced drag coefficient $C_{D_{C_L^2}}$ was then obtained from the cross plots of C_D against ΔC_L^2 (fig. 9). These results are summarized in figures 10(a), (b), and (c). The flagged symbols on the minimum-drag summary (fig. 10(a)) denote values of C_D taken from the time history whenever $|C_L| \leq 0.03$.

The induced-drag summary plot (fig. 10(c)) indicates $C_{D_{C_L^2}}$ was substantially less than $\frac{1}{57.3 C_{L_{\alpha_{low lift}}}}$ at subsonic speeds, but only

slightly less at transonic speeds; at no time did it closely approach the subsonic theoretical minimum $\frac{1}{\pi A}$.

Reference 4 contains no drag data for comparison.

Pitching Moment

The total pitching moment was determined by the two-accelerometer method (ref. 6). The basic data, which include the dynamic moment due to $\dot{\alpha}$ and $\dot{\theta}$, are given as cross plots of total C_m and α_f in figures 11(a) and (b). Although those portions of the curves where the model executed only one-half cycle of oscillation before the stabilizer moved are not as well defined as those where the model did make a complete cycle, it can be seen that at subsonic speeds no single value of static stability can be given, whereas at transonic speeds whenever the amplitude of the motion is large enough as at $M = 1.26, 1.24$, and 1.02 , two distinct slopes can be discerned. The stability derivative $C_{m\alpha}$ and the aerodynamic-center location are given in figures 12(a) and (b). The angle-of-attack range for the various stability levels, including the pitch-up boundary, are given in figure 12(c). The only available data for comparison, (ref. 4) indicate an increase in stability with increasing angle of attack at subsonic speeds below the high-lift break, and at the higher transonic speeds no change in stability with increasing angle of attack (fig. 12(b)). Thus, the wind-tunnel data did not predict the change in static stability at moderate lift.

The pitching-moment coefficient at zero angle of attack, $C_{m\alpha_f=0}$, is given for the two stabilizer settings in figure 12(d), from which the stabilizer pitching effectiveness, $C_{m\delta_{\alpha=0}}$, figure 12(e) was derived.

The corresponding data from reference 4 are also shown in figures 12(d) and (e).

Wing Bending Moment

The wing bending-moment data, obtained from a strain gage mounted 34.4 percent of the total semispan outboard of the fuselage center line, have been corrected for inertia effects. These data are shown plotted against fuselage angle of attack in figures 13(a) and (b) without regard for the position of the stabilizer. It is apparent that, as for lift, the slope increases with increasing angle of attack. These slopes and the angle-of-attack range over which they apply are given in figures 14(a) and (b). Also, it should be noted that near the high-angle-of-attack end

of the subsonic curves, for example, $M = 0.86$ (fig. 13(a)) the C_{BM} remains substantially constant for large increases in α . These maximum bending-moment coefficients are summarized in figure 14(c) along with $C_{BM_{\alpha=0}}$. As mentioned in the section entitled "Instrumentation," this bending moment was primarily obtained to aid in the buffet study, and since the lift on the portion of the wing outboard of the strain gage was not measured separately, it is not possible to determine the lateral center of pressure.

Buffet Boundaries

At several times during the flight, high frequency oscillations appeared on the telemeter traces of the wing bending-moment strain gage and the accelerometers. The predominant frequency of these oscillations was 80 cycles per second or about the natural frequency of first wing-body bending mode (see fig. 1(d)) and it was judged that at subsonic speeds the model was being shaken by buffet arising from flow separation over the wing.

The onset of buffet was determined from inspection of the telemeter traces of wing bending moment and the normal acceleration at the center of gravity and at the pilot's seat. Part of the telemeter record showing the angle of attack and wing bending-moment traces is shown in figure 15. It was considered that the buffet had started at that point where the character of the trace was significantly changed by the appearance of a variable-amplitude 80-cycles-per-second oscillation. These points, indicated in figures 15(c), (d), (e), and (f), are shown in figures 16(a) and (b) as boundaries of fuselage angle of attack and lift coefficient. Similarly derived points from the normal-acceleration time histories, where the detectable half amplitude of the oscillation was on the order of $\pm 0.3g$ units ($\Delta C_N = \pm 0.033, 0.016, \text{ and } 0.009$ at $M = 0.5, 0.7, \text{ and } 0.9$) are shown in figures 16(a) and (b).

The dynamic response of the pilot's seat in the actual airplane will probably be quite different because of the differences in model and airplane construction. Also, the steady-state buffet boundaries may be significantly lower than those presented here, since in this test the model passed through the boundary quickly, and in some cases the bending-moment coefficient levelled off for an appreciable time before detectable buffet oscillations appeared. (See again fig. 15(c).) The boundary obtained from the time history of the actual airplane pilot's seat normal acceleration (ref. 4) is also shown in figure 16.

At transonic speeds a buffet-like phenomenon was encountered near $M = 1.21$ at $\alpha_F = 2.0^\circ$ (fig. 15(a)) and $M = 1.08$ at $\alpha_F = -1.1^\circ$ (fig. 15(b)). It is not known if this phenomenon is actually wing buffet.

However, it is known that between $T = 0$ and about 4.5 seconds the model was within a layer of air the lapse rate of which closely approached the dry adiabatic 5.5° R per 1,000 feet (fig. 4). The model then penetrated and emerged from a transition layer characterized by a mild temperature inversion and rapidly changing wind direction. The remainder of the flight took place in a layer of air whose temperature lapse rate was approximately that of the moist adiabatic, 2.5° R per 1,000 feet.

It seems probable that mild turbulence would be associated with such an atmospheric discontinuity, and this turbulence may well have excited the wing-body first bending mode. The resulting variations in wing-root bending moment would be similar to true buffet. An unpublished analysis shows a marked correlation of the appearance of such buffet-like phenomena with rough-air experience of other rocket models.

General Comments on Pitch-Up and Associated Phenomena

The boundaries defining the low-lift break in slope of lift, pitching moment, and bending moment, and the boundaries defining the high-lift break in lift and bending moment, and the pitch-up and buffet boundaries are all given together in figure 17 for convenience. These general results are apparent:

1. Lift and bending moment became nonlinear at the same angle of attack at both low and high lifts.
2. At transonic speeds the static stability increased above the low lift boundary; however, at subsonic speeds the static stability decreased continuously from the lower test limit to the pitch-up boundary.
3. The pitch-up boundary and the boundaries defining the high-lift break in lift and bending moment were substantially the same; however, the buffet boundary did not follow this curve very closely.

SUMMARY OF RESULTS

The detailed results derived from the flight test of a model approximating the McDonnell F3H-1N airplane configuration while the model was decelerating in free flight from a Mach number of 1.27 to 0.40 are given in the figures; some general comments concerning these results follow:

1. The pitch-up boundary and the boundaries defining the high-lift break in lift and bending moment were substantially the same; the buffet boundary, however, did not follow this boundary very closely.

~~CONFIDENTIAL~~


2. Below the high-lift break, the lift-curve slope and wing-root bending-moment slope increased with angle of attack throughout the Mach number range, whereas the static stability decreased with angle of attack at subsonic speeds and increased with angle of attack at transonic speeds.

Langley Aeronautical Laboratory,
National Advisory Committee for Aeronautics,
Langley Field, Va., January 3, 1956.

Norman L. Erskill

Norman L. Crabill
Aeronautical Research Scientist

Approved:

1: 
Joseph A. Shortal
Chief of Pilotless Aircraft Research Division

rwh

~~CONFIDENTIAL~~

APPENDIX

SYMBOLS

A	wing aspect ratio
A_L	acceleration parallel to fuselage center line, g units
A_N	acceleration perpendicular to fuselage center line, g units
A_T	acceleration perpendicular to plane of symmetry, g units
\bar{c}	wing mean aerodynamic chord
C_{BM}	wing bending-moment coefficient, $\frac{\text{Bending moment}}{q \frac{S}{2} \frac{b}{2}}$
C_c	chord-force coefficient, $\frac{A_{L_{cg}} W}{qS}$
C_D	drag coefficient, $C_N \sin \alpha_F - C_c \cos \alpha_F$
C_L	lift coefficient, $C_N \cos \alpha_F + C_c \sin \alpha_F$
ΔC_L	$C_L - (C_L \text{ for } C_{D_{min}})$
C_m	pitching-moment coefficient about the center of gravity, $\frac{\text{Pitching moment}}{qS\bar{c}}$
C_N	normal-force coefficient, $A_{N_{cg}} \frac{W}{qS}$
C_Y	lateral-force coefficient, $A_T \frac{W}{qS}$
g	acceleration due to gravity
I_y	mass moment of inertia of model in pitch

I_z	mass moment of inertia of model in yaw
M	free-stream Mach number
P_o	free-stream static pressure
q	free-stream dynamic pressure, $0.7P_oM^2$
R	Reynolds number based on \bar{c}
$^{\circ}R$	free-stream static temperature, deg Rankine
S	model wing area
T	time, sec
V	free-stream velocity
V_w	wind velocity
W	weight of model
α_f	angle of attack of fuselage reference at the center of gravity
γ	flight-path angle
θ	angle of fuselage center line relative to fixed reference
δ	deflection of horizontal stabilizer relative to fuselage reference

Subscripts:

av	average
cg	center of gravity
max	maximum
min	minimum
N	nose
t	trim

°°°
°°°
°°°
°°°
°°°
°°°

Derivatives with respect to a quantity are indicated as shown in the following example:

$$C_{m\alpha} = \frac{dC_m}{d\alpha}$$

REFERENCES

1. Crabill, Norman L.: The Effects of Extensible Rocket Racks on Lift, Drag, and Stability of a 1/10-Scale Rocket-Boosted Model of the McDonnell XF3H-1 Airplane for a Mach Number Range of 0.60 to 1.34 - TED No. NACA DE 351. NACA RM SL53F15, Bur. Aero., 1953.
2. Crabill, Norman L., and McFall, John C., Jr.: Summary of the Lift, Drag, and Stability of 1/10-Scale Rocket-Boosted Models of the McDonnell XF3H-1 Airplane for a Mach Number Range of 0.6 to 1.4 As Affected by the Operation of Extensible Rocket Racks - TED No. NACA DE 351. NACA RM SL54A18, Bur. Aero., 1954.
3. Gillis, Clarence L., Peck, Robert F., and Vitale, A. James: Preliminary Results From a Free-Flight Investigation at Transonic and Supersonic Speeds of the Longitudinal Stability and Control Characteristics of an Airplane Configuration With a Thin Straight Wing of Aspect Ratio 3. NACA RM L9K25a, 1950.
4. Miller, C. W.: Aerodynamic Data Concerning Model F3H-1N Free-Flight Rocket Model. Rep. No. 3484 (Contract NOa(s)-51-640), McDonnell Aircraft Corp., Apr. 5, 1954.
5. Carter, Howard S., and Merlet, Charles F.: Flight Determination of the Pressure Recovery and Drag Characteristics of a Twin Side-Inlet Model at Transonic Speeds. NACA RM L53E05, 1953.
6. Vitale, A. James: Effects of Wing Elasticity on the Aerodynamic Characteristics of an Airplane Configuration Having 45° Sweptback Wings As Obtained From Free-Flight Rocket-Model Tests at Transonic Speeds. NACA RM L52L30, 1953.

0000000000

TABLE I

PHYSICAL CHARACTERISTICS OF THE TEST MODEL

14

Mass characteristics:

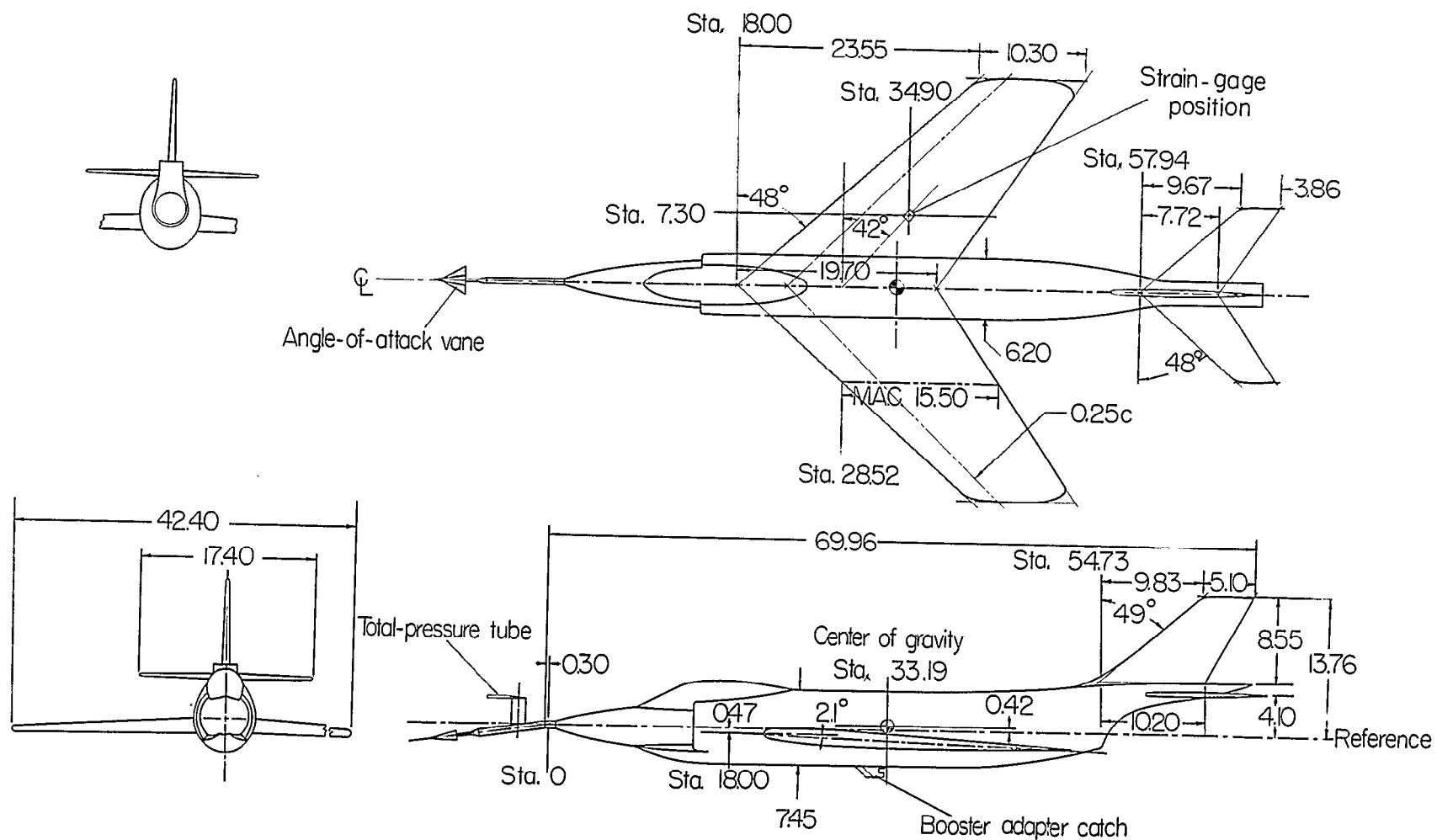
Center-of-gravity location:

Longitudinal, percent M.A.C. aft of L.E.	30.1
Vertical, in. above reference	0.42
Weight, lb	137.8
Wing loading, lb/sq ft	31.18
Moments of inertia:	
I_Y , slug-ft ²	7.23
I_Z , slug-ft ²	7.73

Geometrical characteristics:

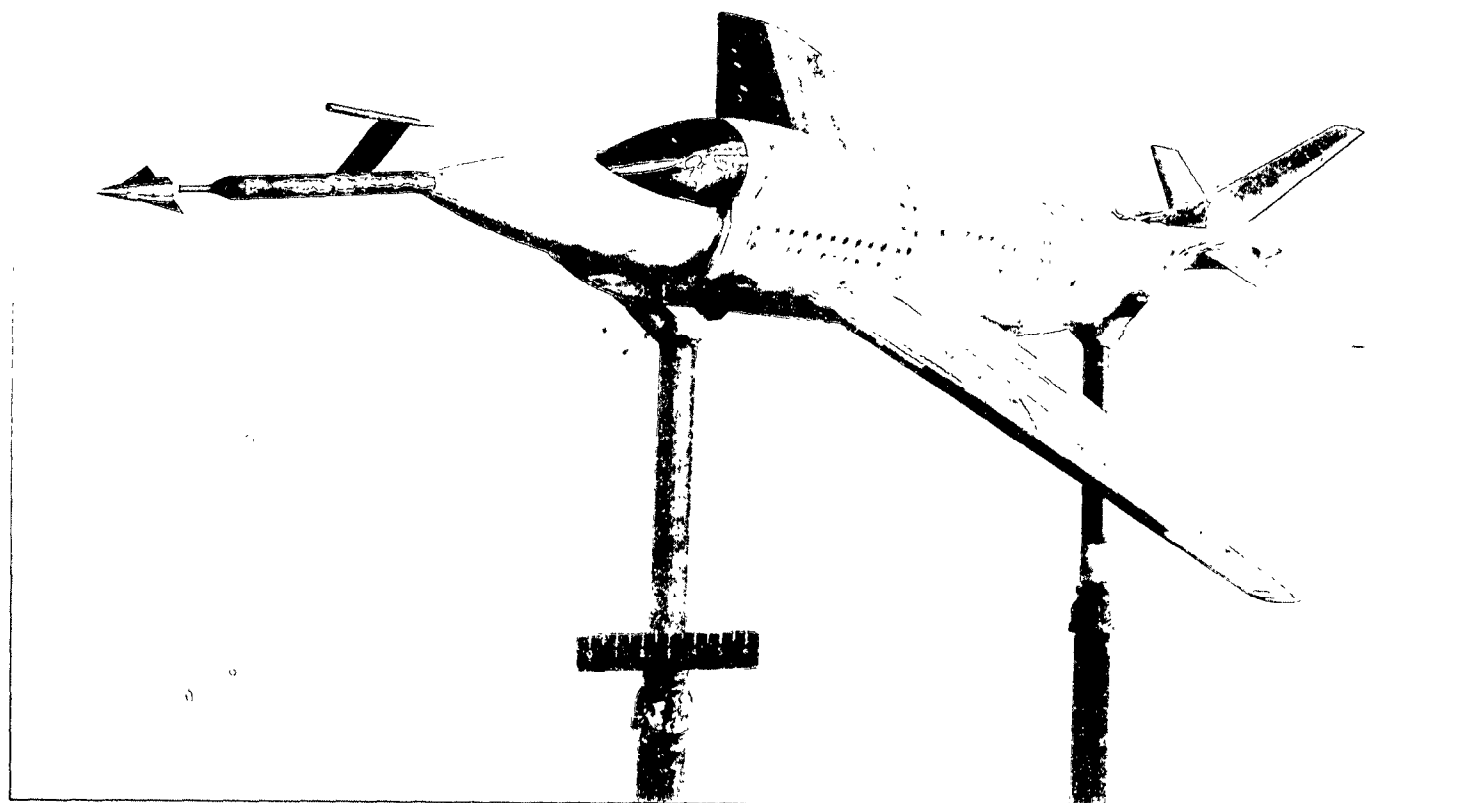
	<u>Wing</u>	<u>Stabilizer</u>	<u>Fin</u>
Aspect ratio	2.82	3.00	1.118
Sweepback of quarter-chord line, deg	45.0	45.0	45.0
Taper ratio	0.523	0.50	0.50
Incidence, deg	2.0	1 to -3	0
Dihedral	0	0	0
Area (total), sq ft	4.42	0.70	(exposed) 0.468
Span	3.533 ft	17.40 in.	8.550 in.
Root chord (center line), in.	19.70	7.72	10.200
Tip chord, in.	10.30	3.86	5.100
Mean aerodynamic chord, in.	15.501	6.004	7.933
Fuselage station of vertex, in.	18.00	57.94	54.730
Fuselage station of L.E. of M.A.C., in. . .	28.519	62.236	59.10
Spanwise station of M.A.C., in.	9.47	3.866	
Airfoil section at root	NACA 0008.6-1.08	NACA 0007-1.16	NACA 0007-1.16
	41/1.20	38/1.14	38/1.14 mod.
Airfoil section at tip	NACA 0006.4-1.16	NACA 0007-1.16	NACA 0007-1.16
	38/1.14	38/1.14	38/1.14 mod.

NACA RM SL56A13



(a) Three-view drawing of the test model. All dimensions are in inches.

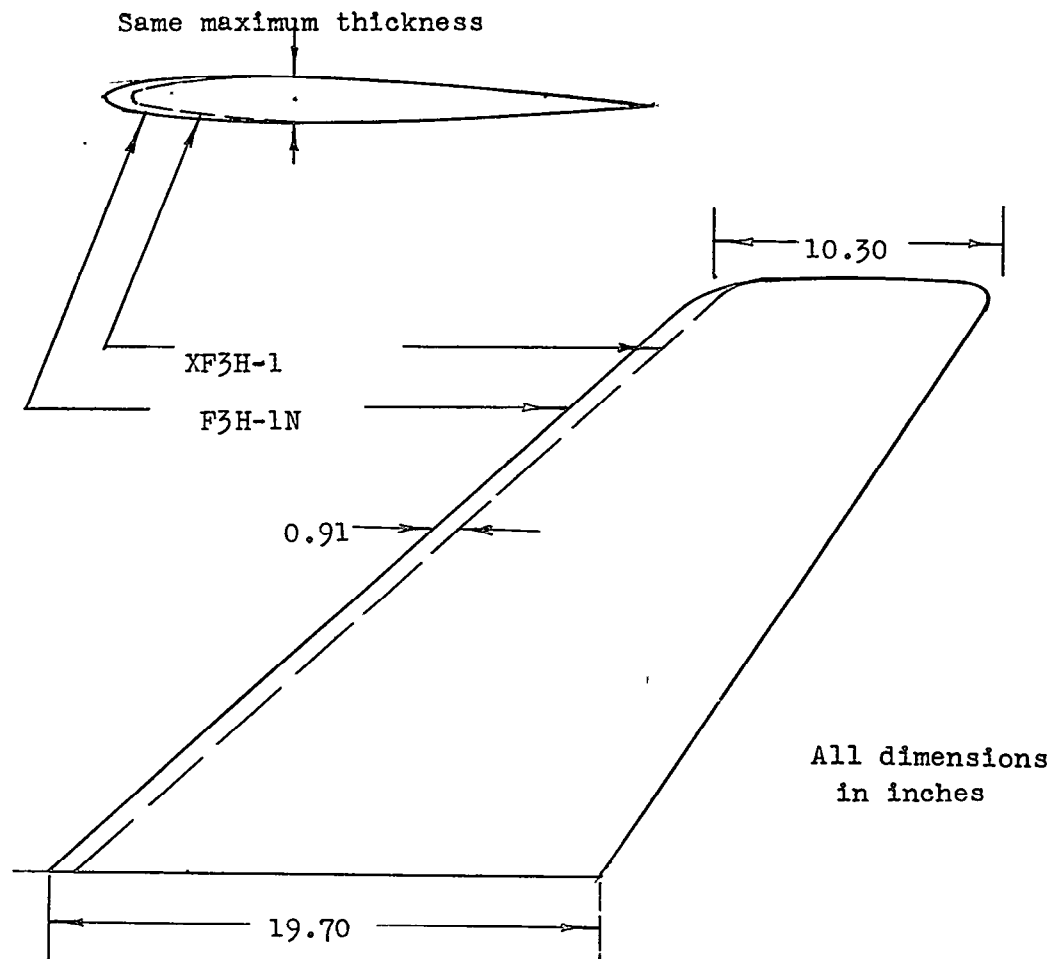
Figure 1.- Model description.



(b) Photograph of the model.

L-87353.1

Figure 1.- Continued.

~~CONFIDENTIAL~~

	XF3H-1	F3H-1N
Aspect Ratio	3.0	2.82
Taper Ratio	0.50	0.524
Sweepback of quarterchord	45	45
Airfoil		
Root	N.A.C.A. 0009-1.16 38/1.14 Modified	N.A.C.A. 0008.6-1.08 41/1.20
Tip	N.A.C.A. 0007-1.16 38/1.14 Modified	N.A.C.A. 0006.4-1.16 38/1.14

(c) Comparison between the XF3H-1 and F3H-1N wings.

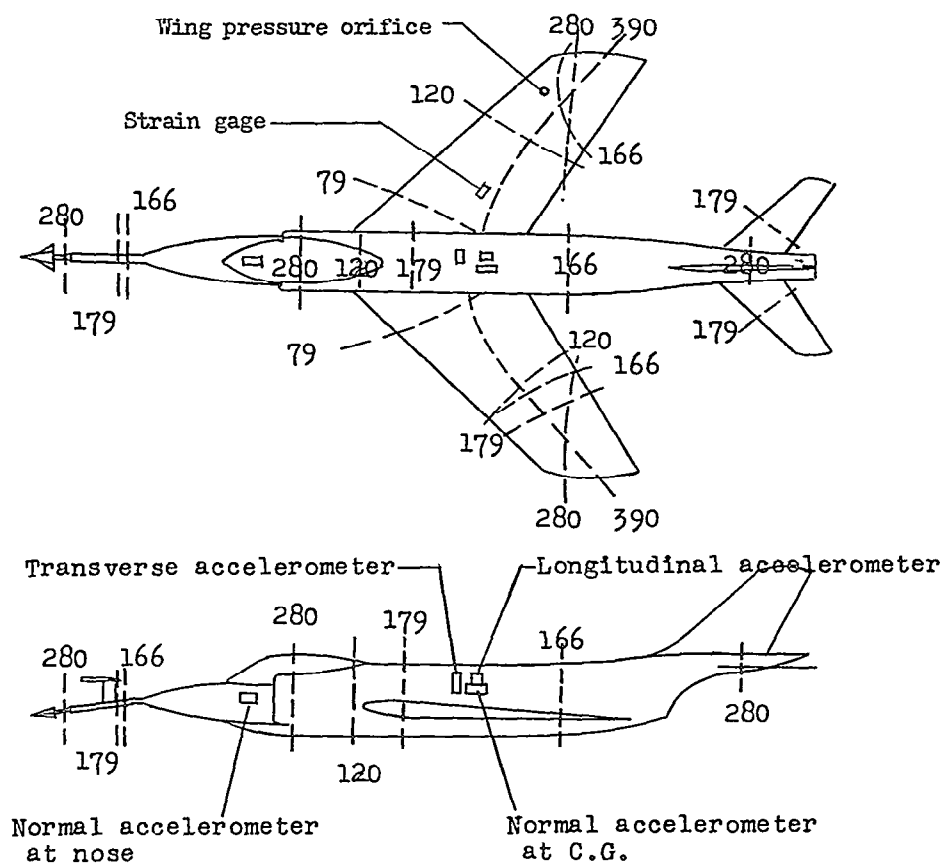
Figure 1.- Continued.

~~CONFIDENTIAL~~

~~CONFIDENTIAL~~

FREQUENCIES OBSERVED ON TELEMETER TRACES WHEN MODEL
COMPONENTS WERE STRUCK

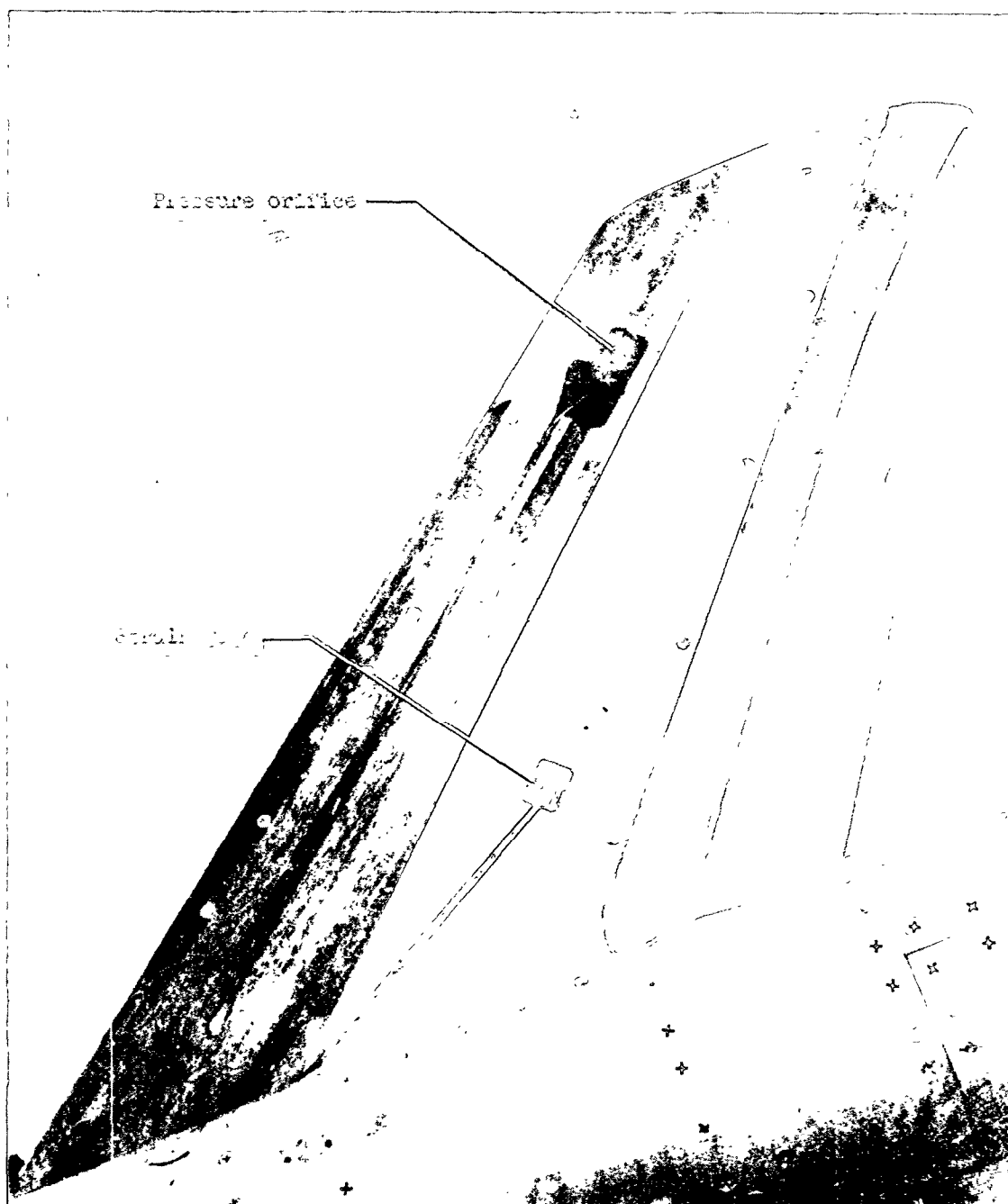
Component struck	Instrument responded at these frequencies, cps				
	AN _{Cg}	AN _N	AL	AT	Strain gage
Left wing		80	80	80	80
Right wing		80	80		79.5
Vertical fin		165		80	80.6
Left horizontal tail	111	100			80
Right horizontal tail		80	82		80
Nose		80			80
		167			



(d) Vibration characteristics of the model.

Figure 1.- Continued.

~~CONFIDENTIAL~~

~~CONFIDENTIAL~~

(e) Photograph of the upper surface of the right wing showing the strain gage and pressure orifice installations. L-87352.1

Figure 1.- Concluded.

~~CONFIDENTIAL~~

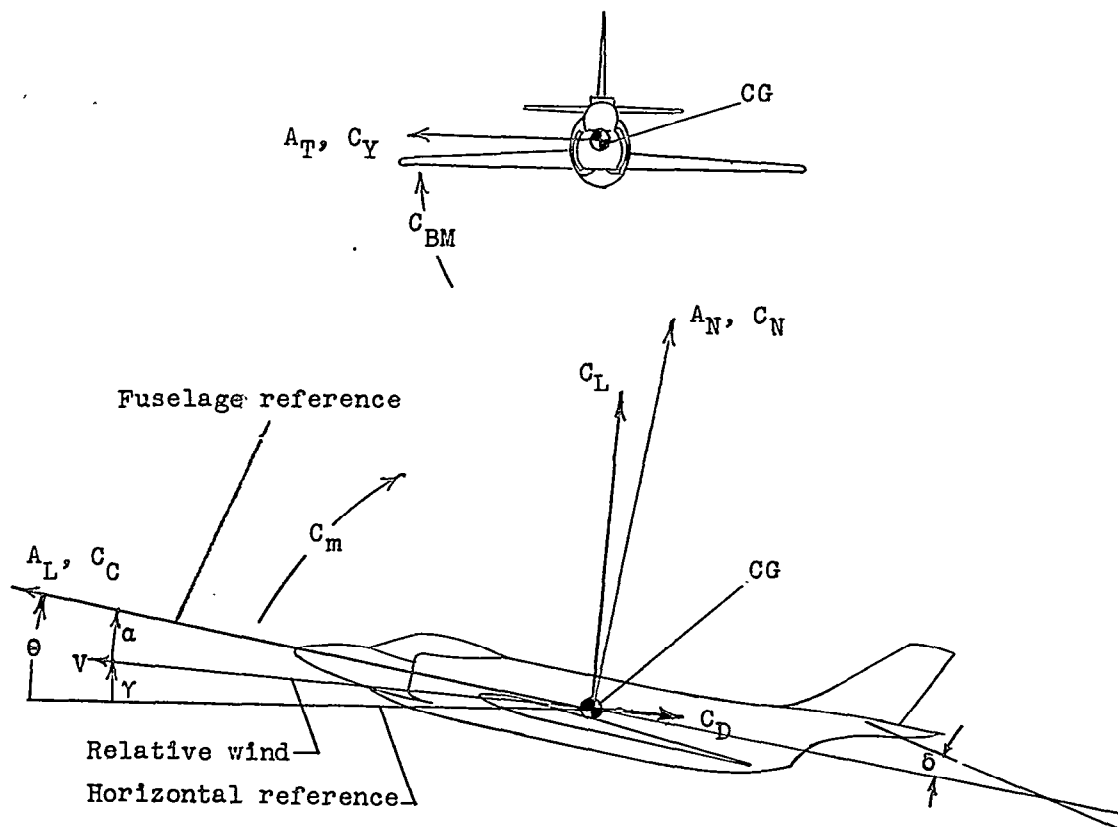
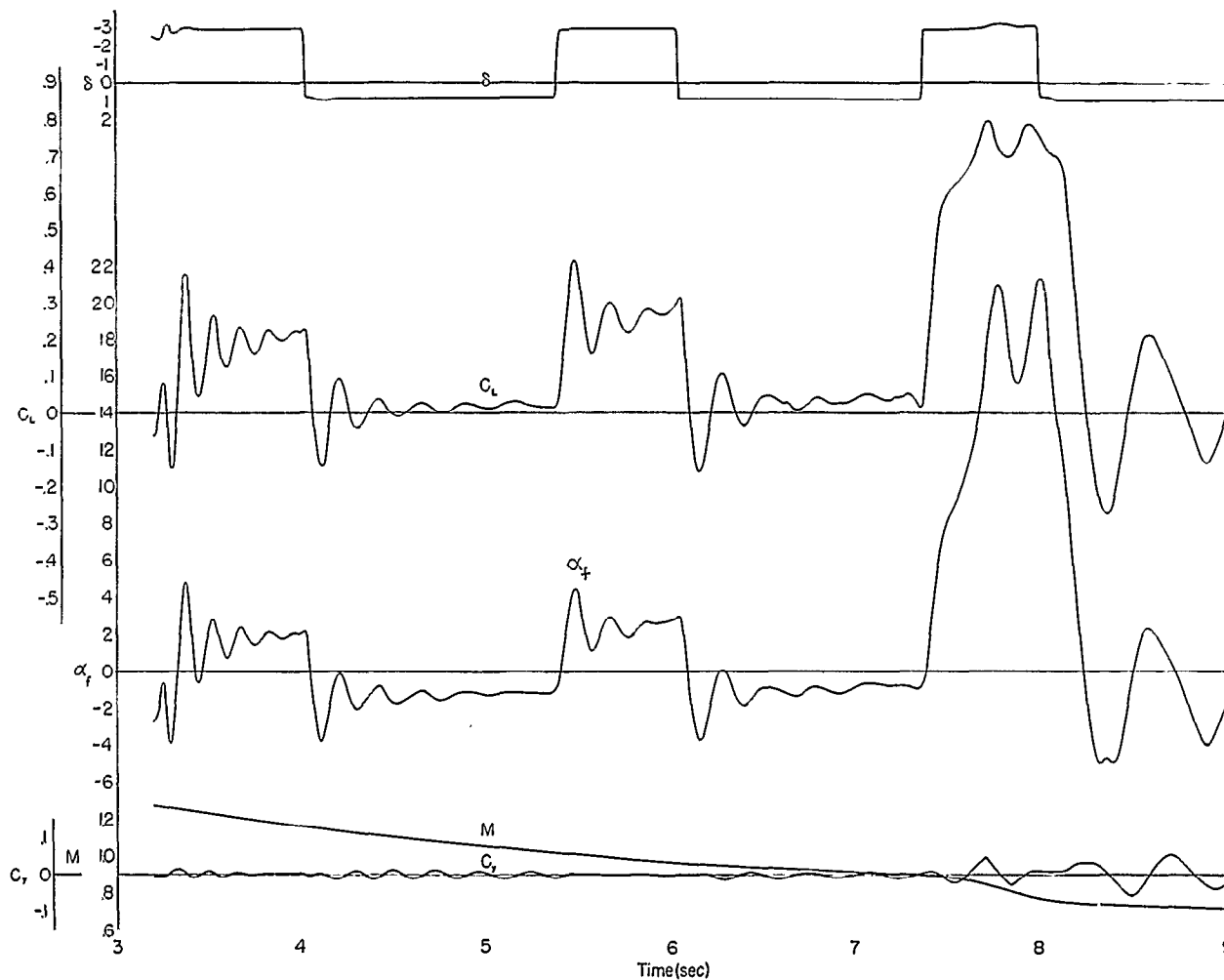
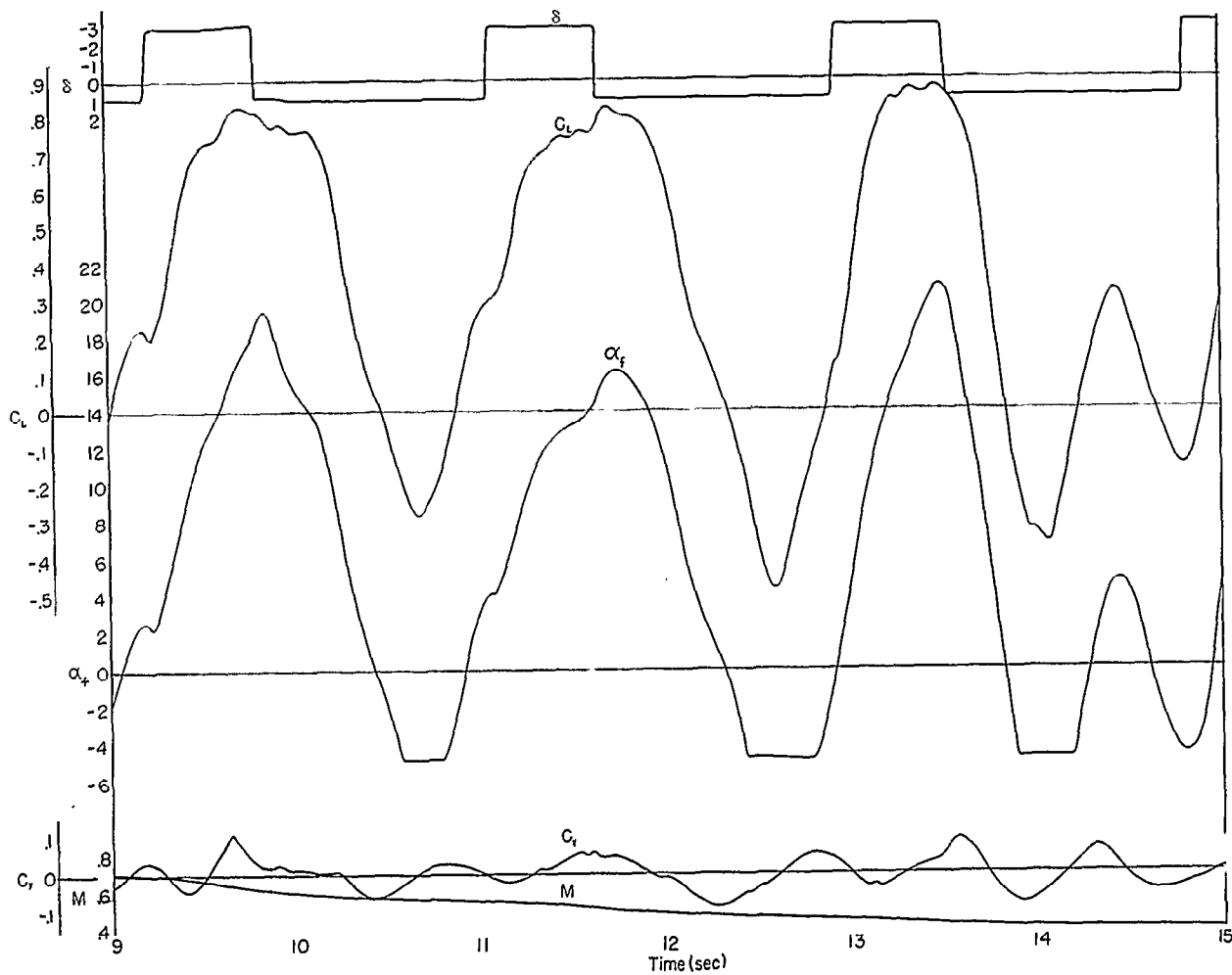


Figure 2.- Positive values of forces, moments, and displacements are indicated by arrows.



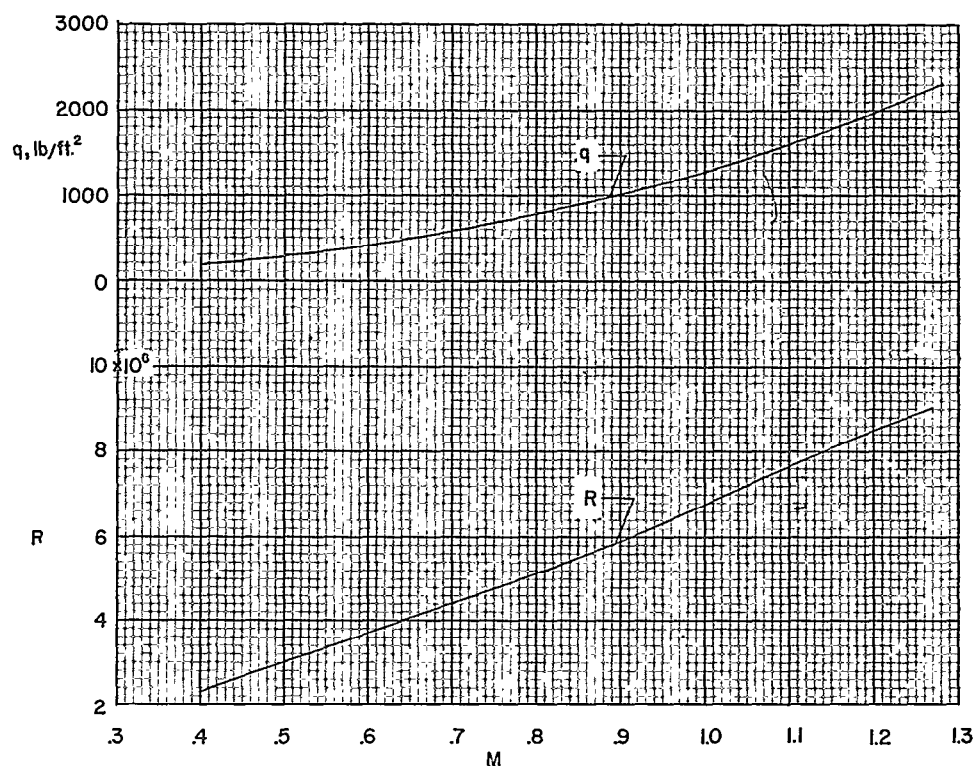
(a) $T = 3.2$ to 9.0 seconds.

Figure 3.- Partial time history.

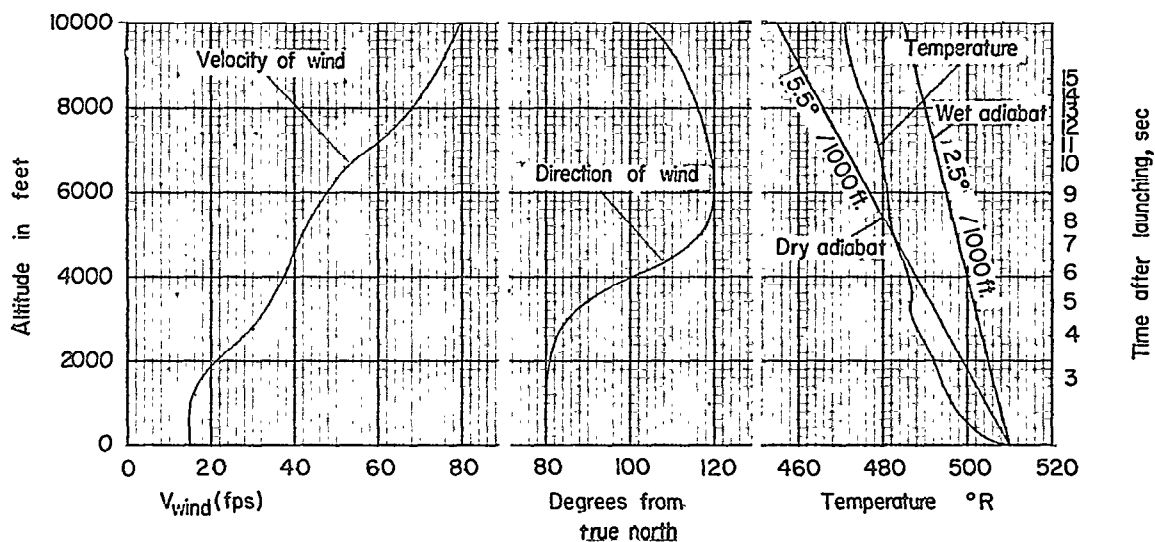


(b) $T = 9.0$ to 15.0 seconds.

Figure 3.- Concluded.

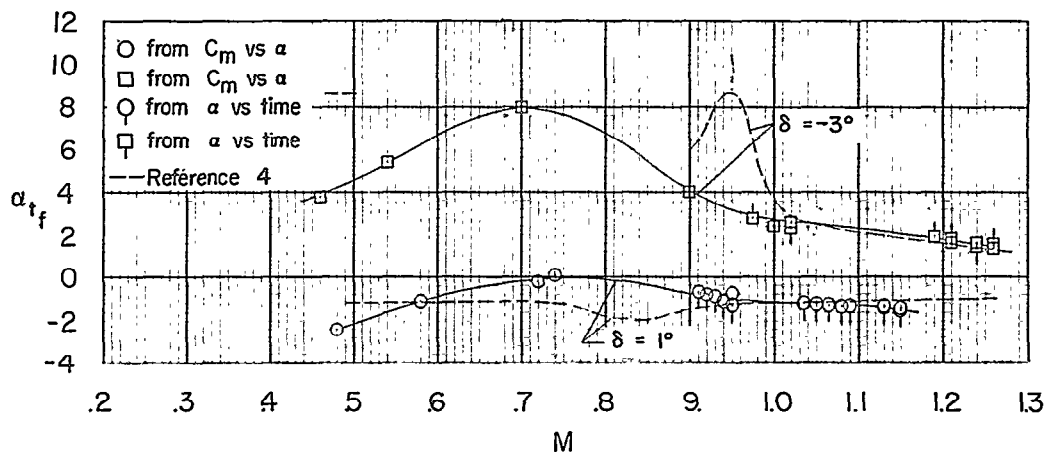


(a) Reynolds number and dynamic pressure.

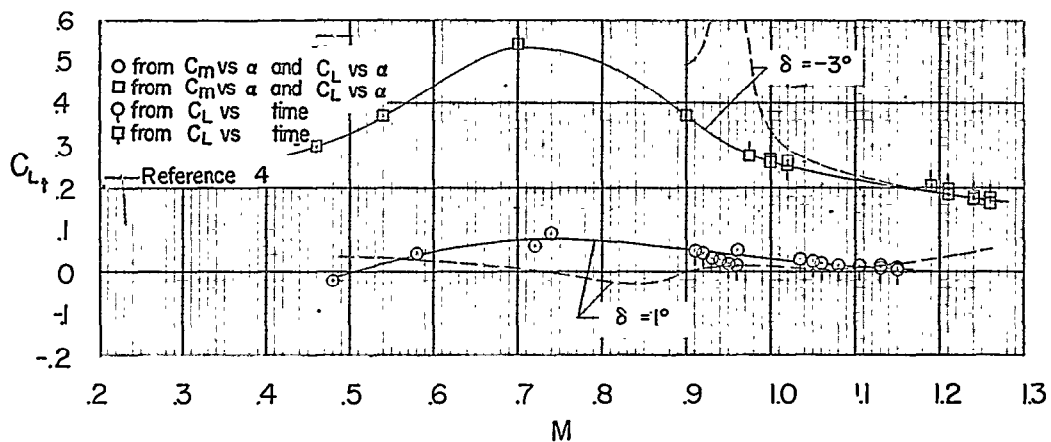


(b) Velocity of wind, direction of wind, and temperature.

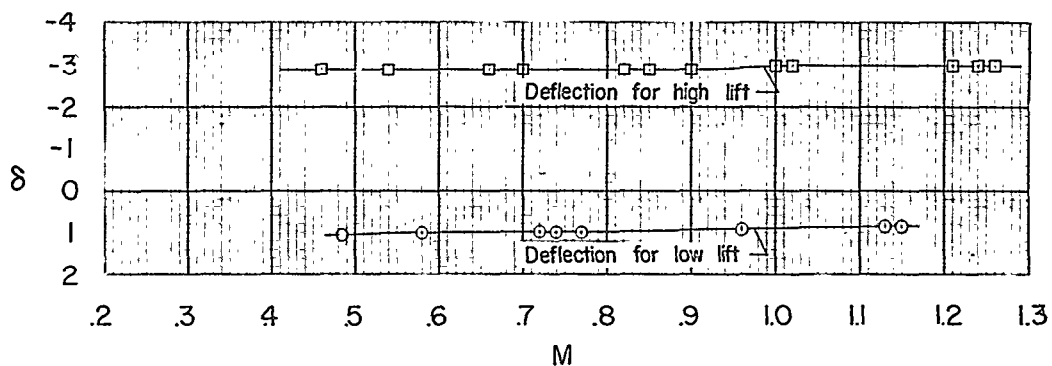
Figure 4.- Test conditions.

~~CONFIDENTIAL~~

(a) Trim angle of attack of fuselage reference.



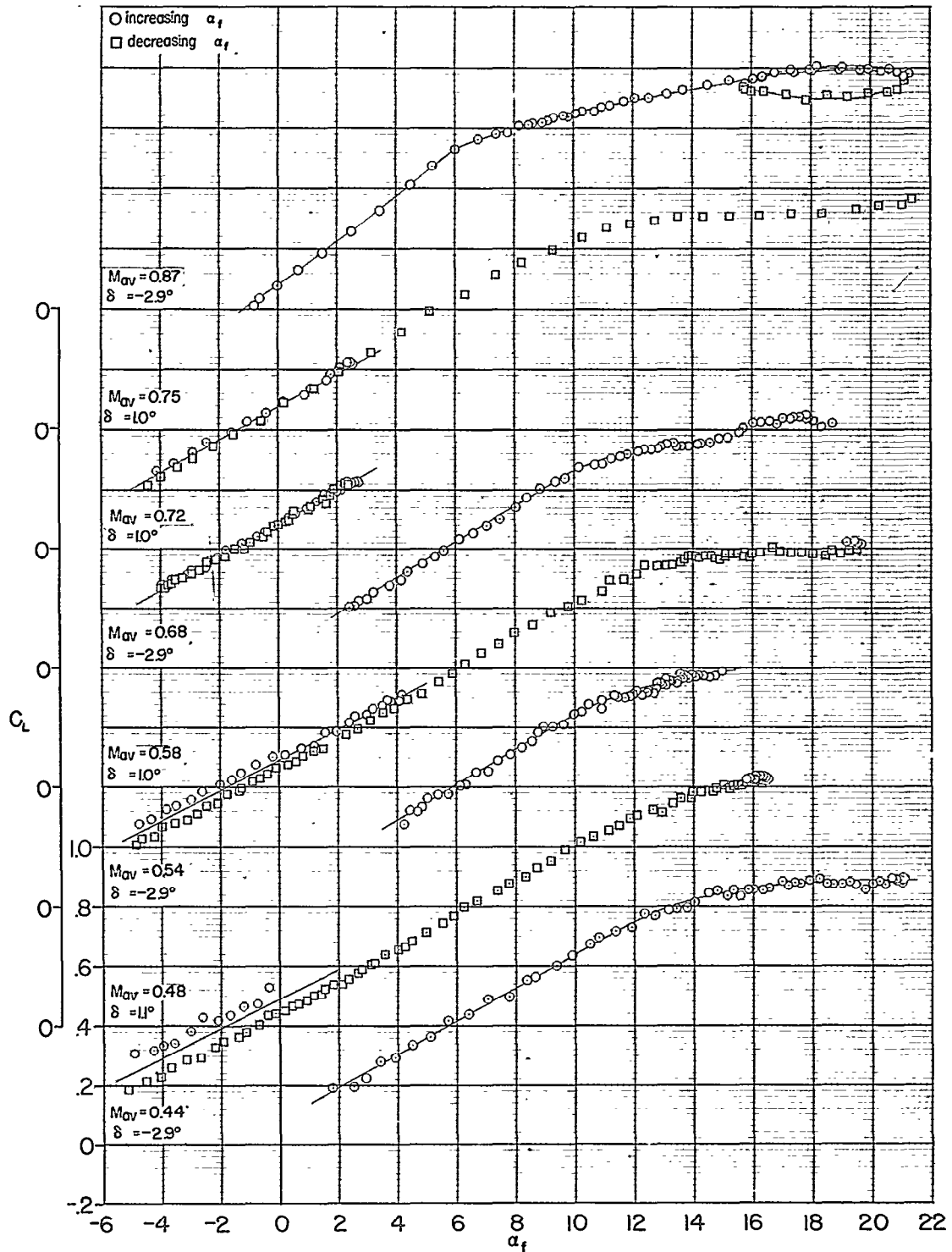
(b) Trim lift coefficient.



(c) Stabilizer incidence relative to fuselage reference.

Figure 5.- Trim characteristics.

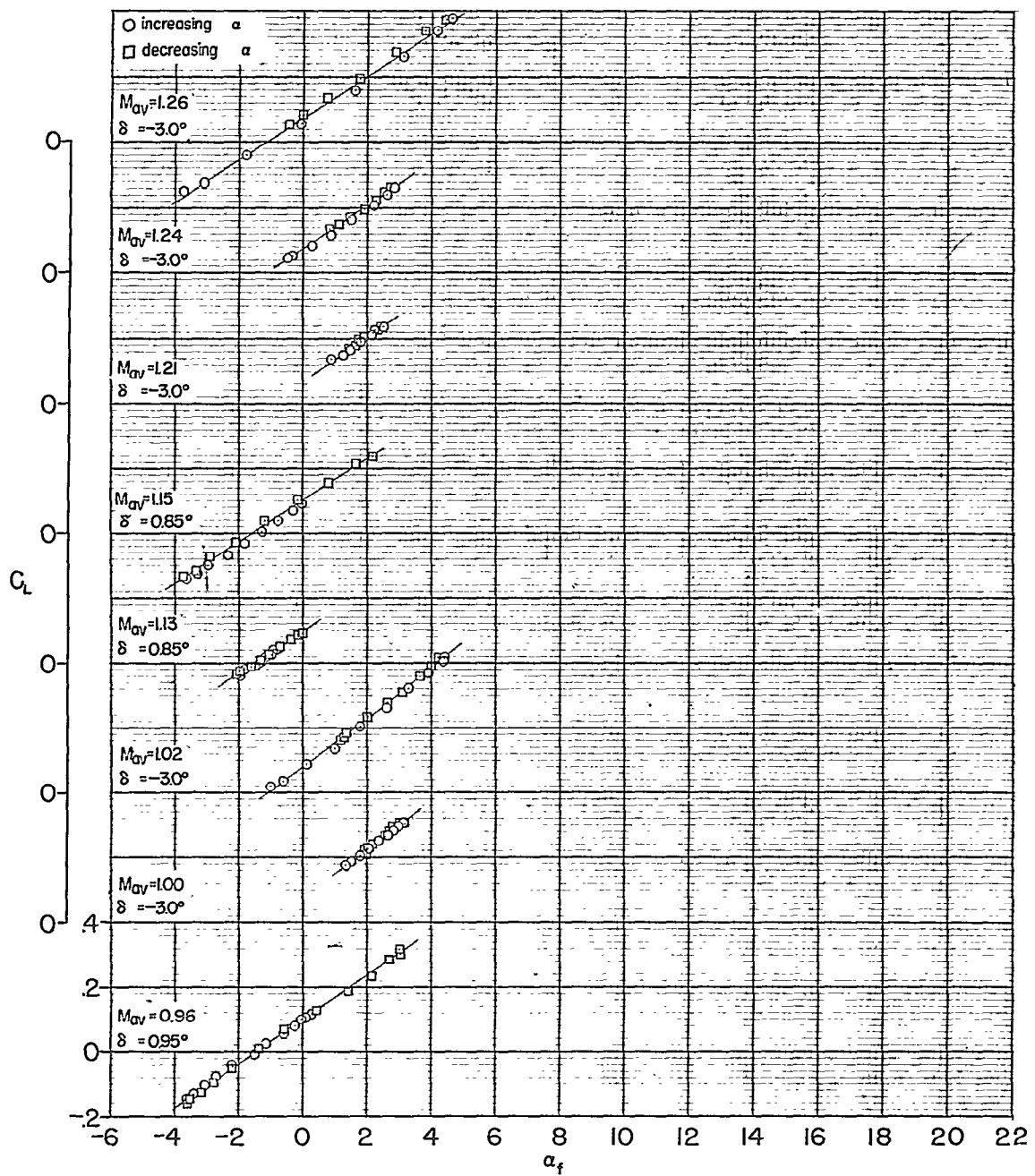
~~CONFIDENTIAL~~

~~CONFIDENTIAL~~

(a) Subsonic speeds.

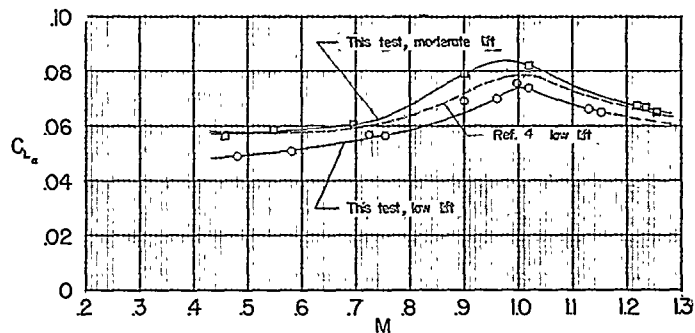
Figure 6.- Basic lift data.

~~CONFIDENTIAL~~

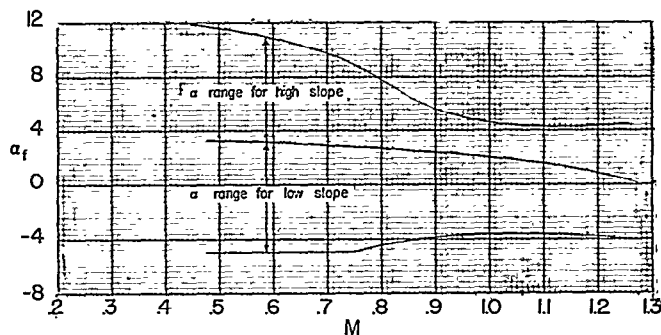


(b) Transonic speeds.

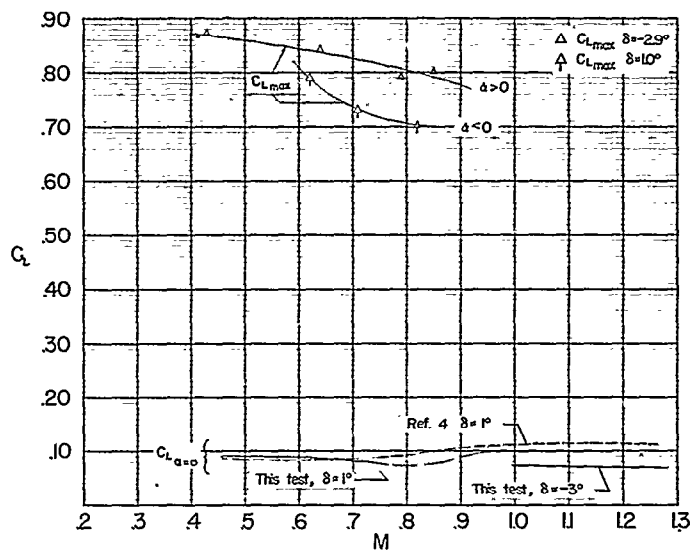
Figure 6.- Concluded.

~~CONFIDENTIAL~~

(a) Lift-curve slope.



(b) Range of angle of attack for which slopes apply.

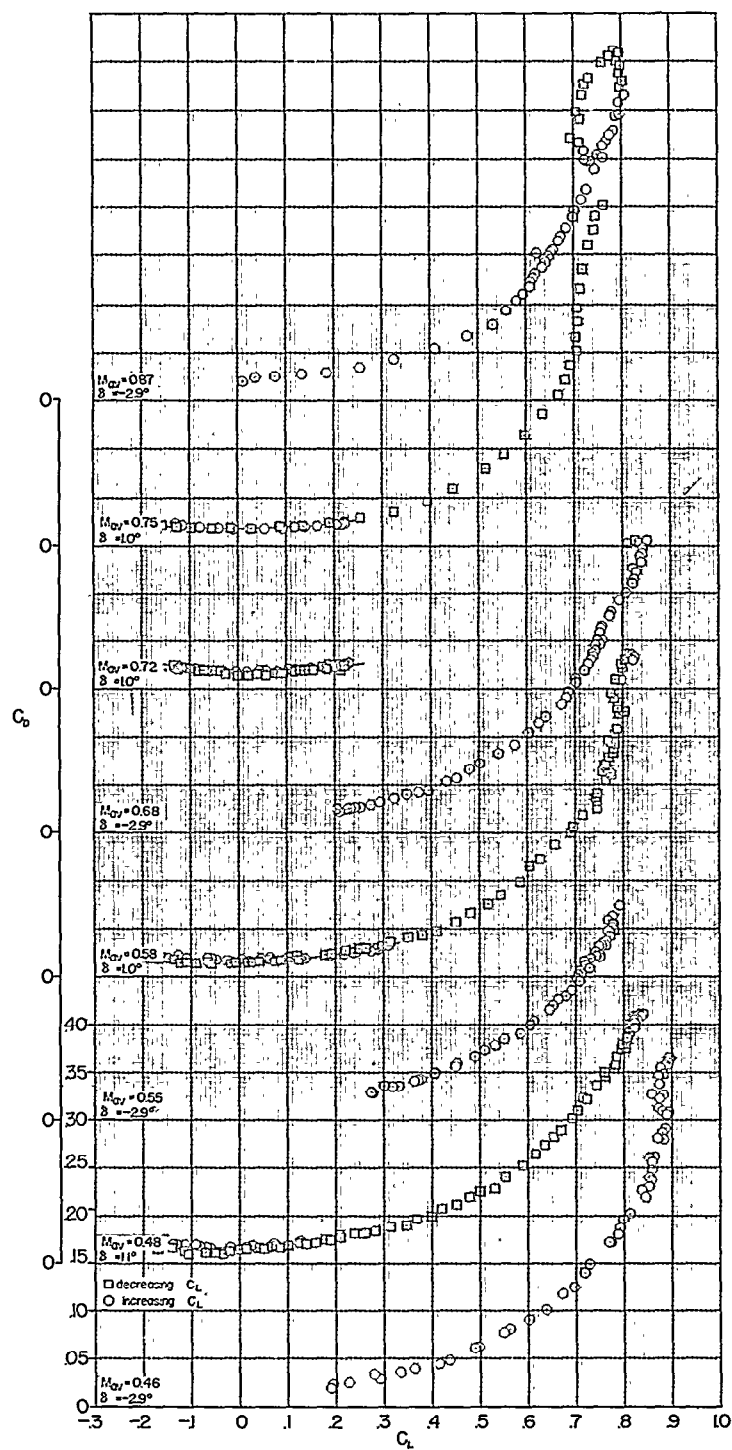


(c) Lift coefficient at zero angle of attack and maximum lift coefficient.

Figure 7.- Lift summary.

~~CONFIDENTIAL~~

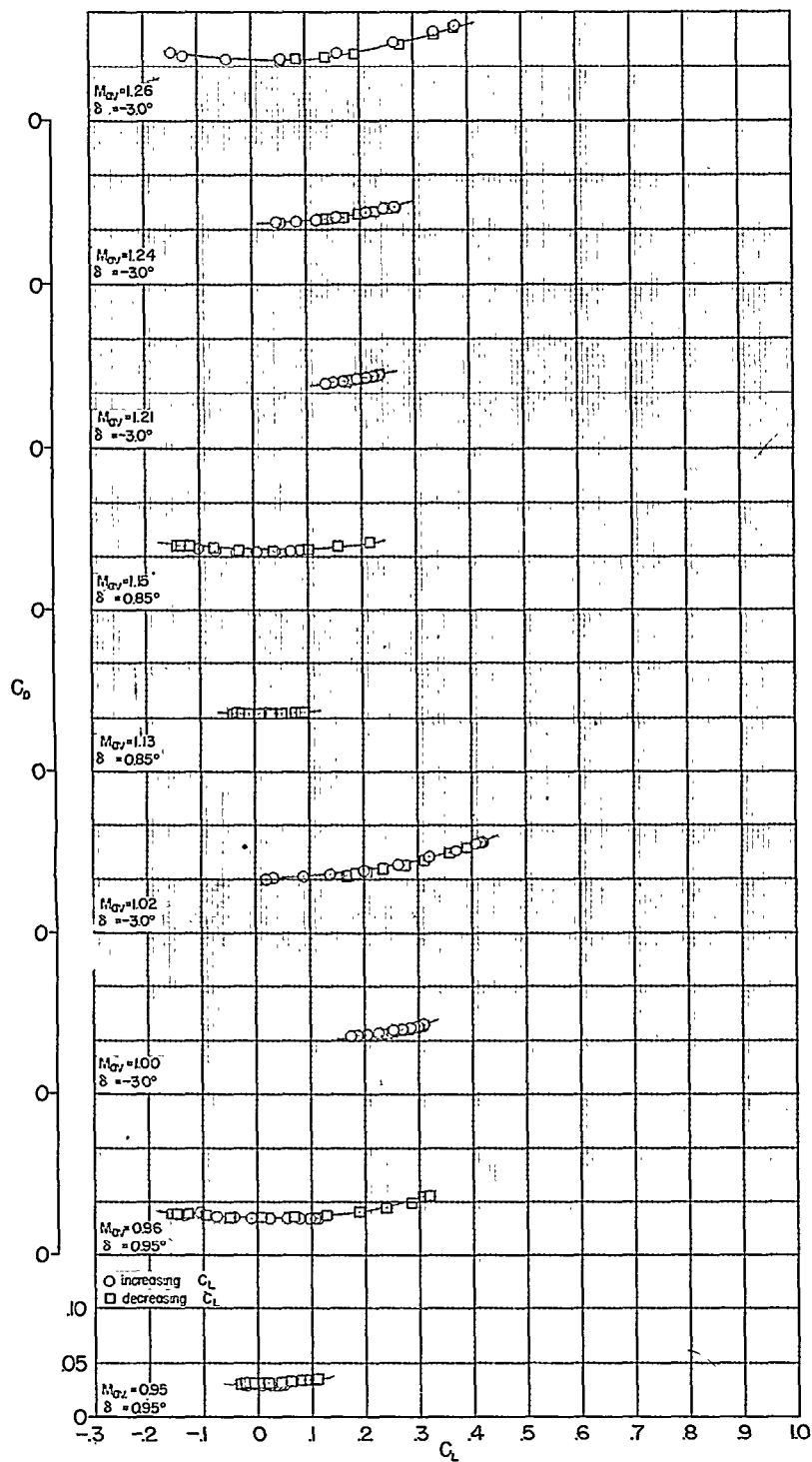
~~CONFIDENTIAL~~



(a) Subsonic speeds.

Figure 8.- Basic drag data.

~~CONFIDENTIAL~~

~~CONFIDENTIAL~~

(b) Transonic speeds.

Figure 8.- Concluded.

~~CONFIDENTIAL~~

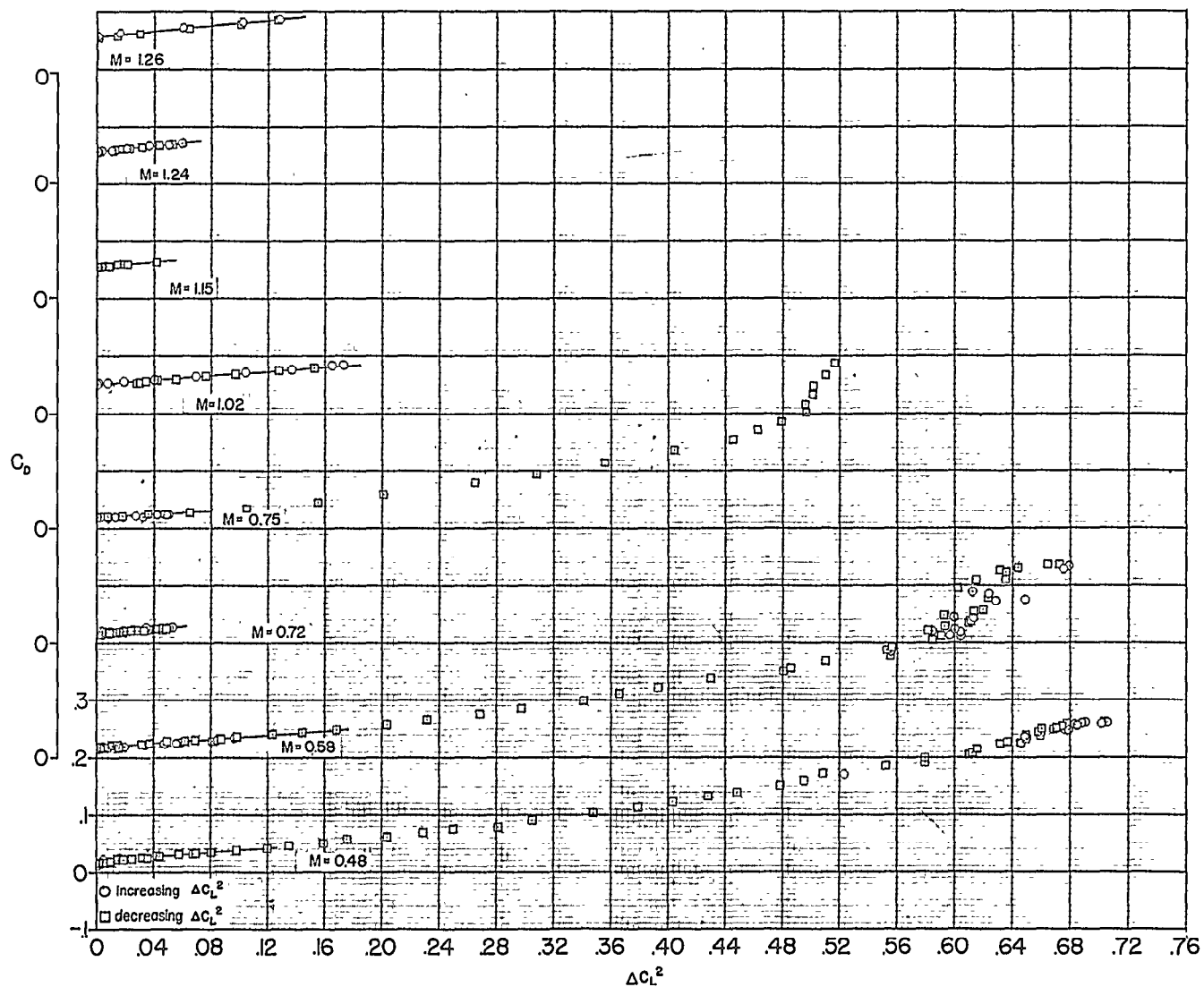
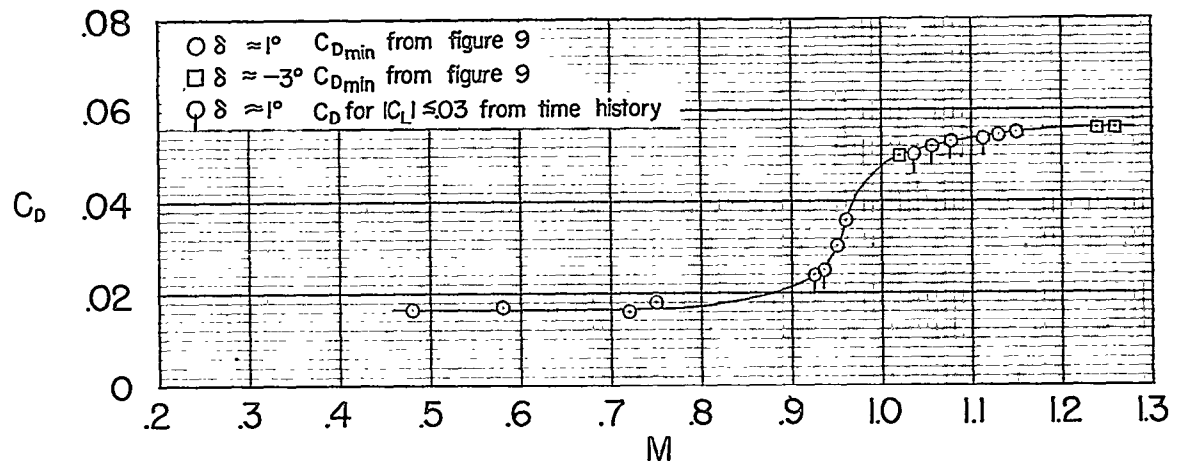
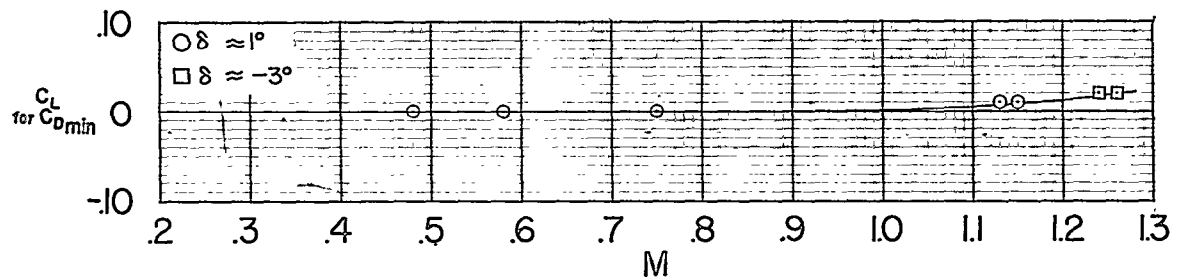


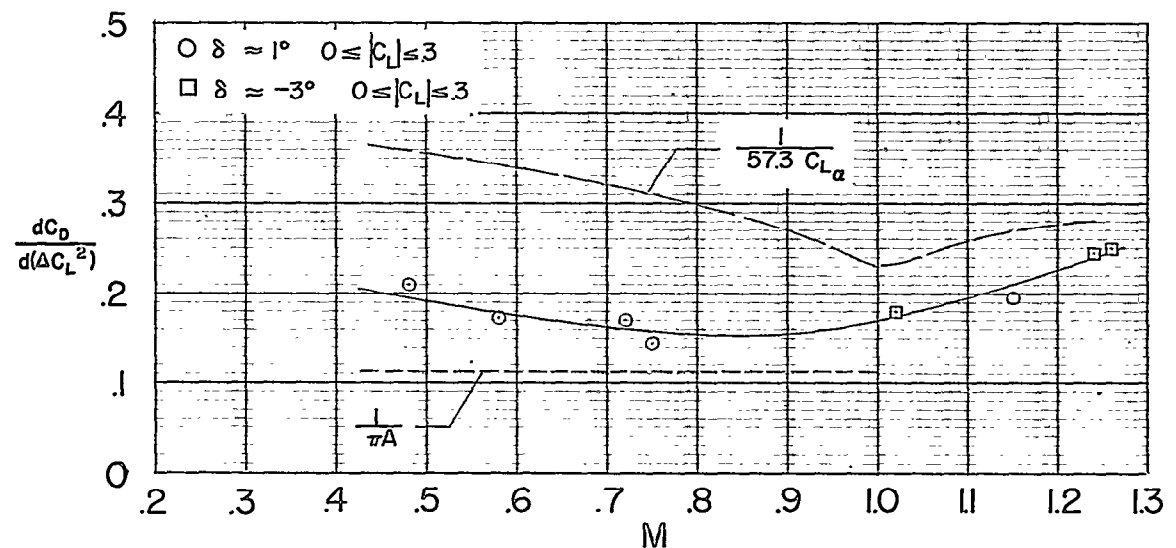
Figure 9.- Induced drag analysis.

~~CONFIDENTIAL~~

(a) Minimum drag coefficient.



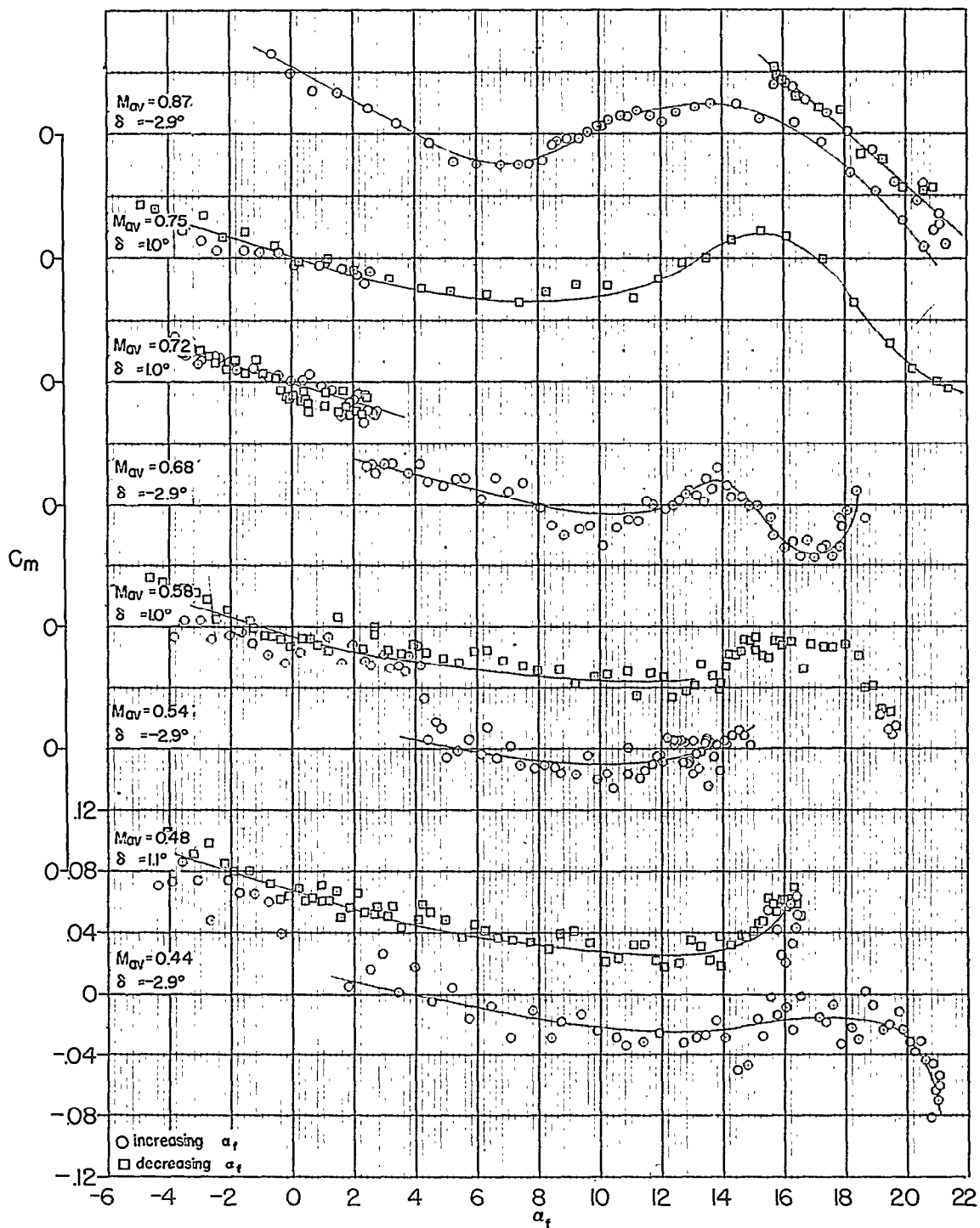
(b) Lift coefficient at minimum drag coefficient.



(c) Induced drag coefficient.

Figure 10.- Drag summary.

~~CONFIDENTIAL~~

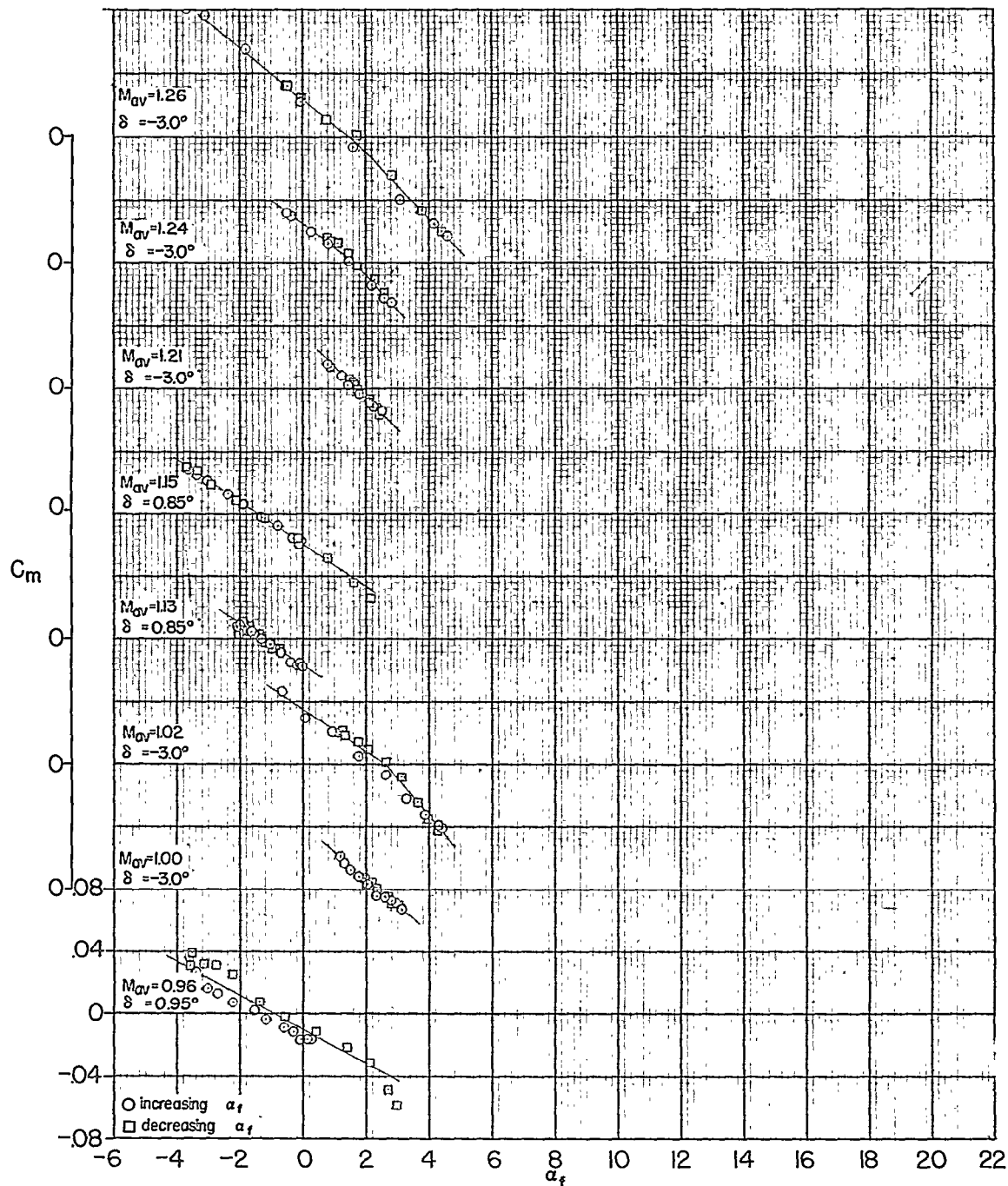
~~CONFIDENTIAL~~

(a) Subsonic speeds.

Figure 11.- Basic pitching-moment data.

~~CONFIDENTIAL~~

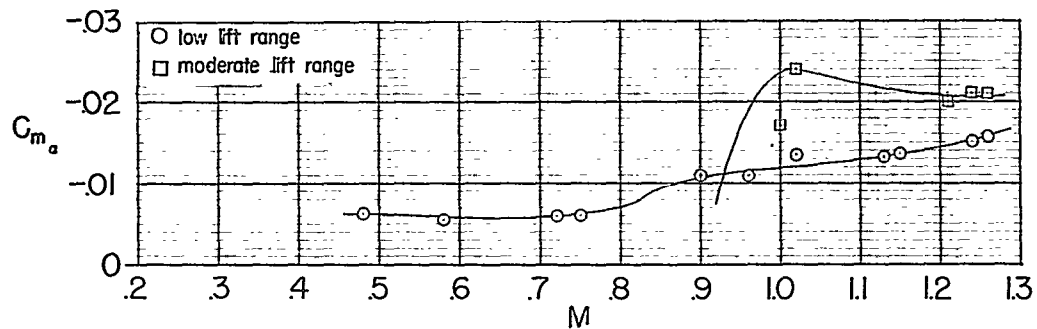
~~CONFIDENTIAL~~



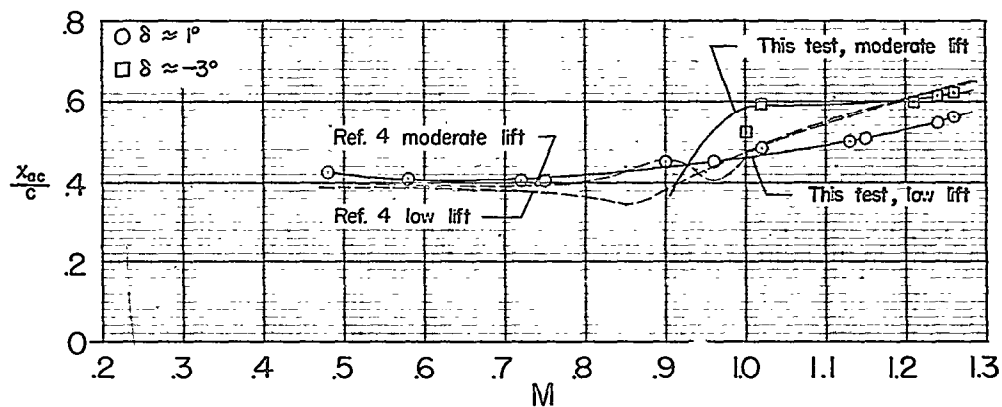
(b) Transonic speeds.

Figure 11.- Concluded.

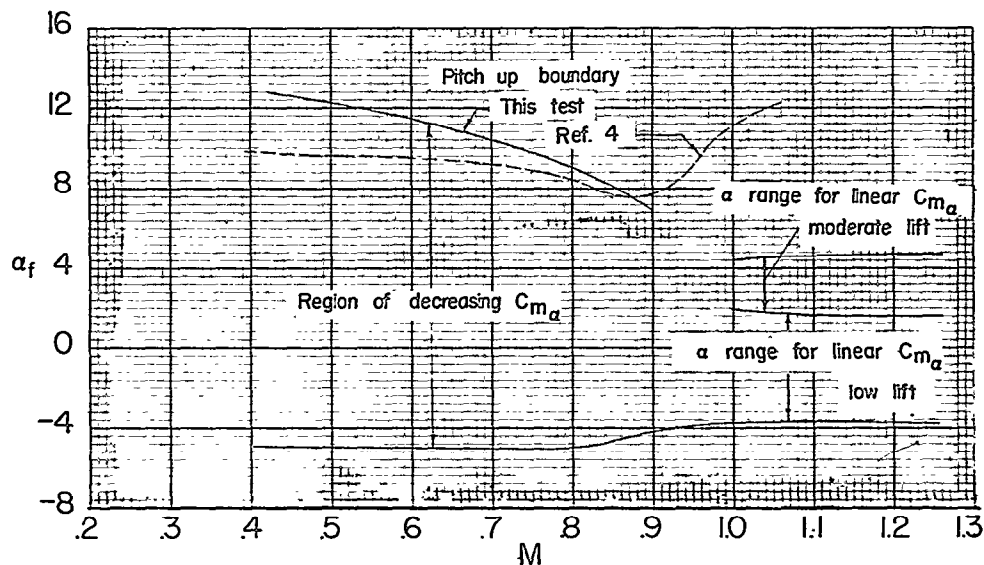
~~CONFIDENTIAL~~



(a) Static stability derivative.

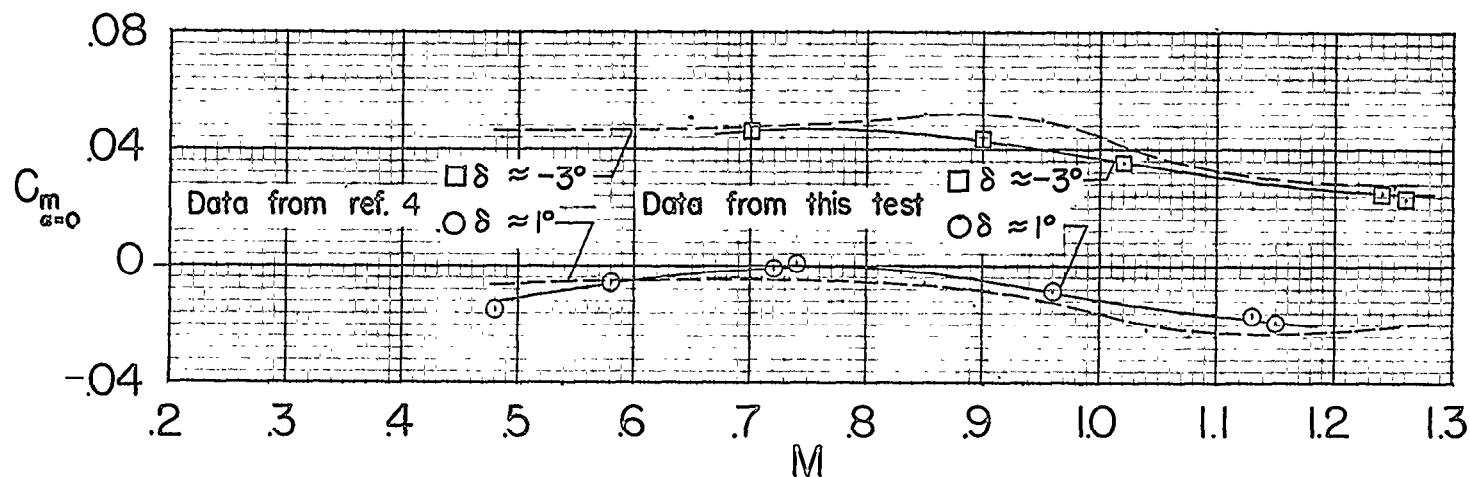


(b) Aerodynamic center location.

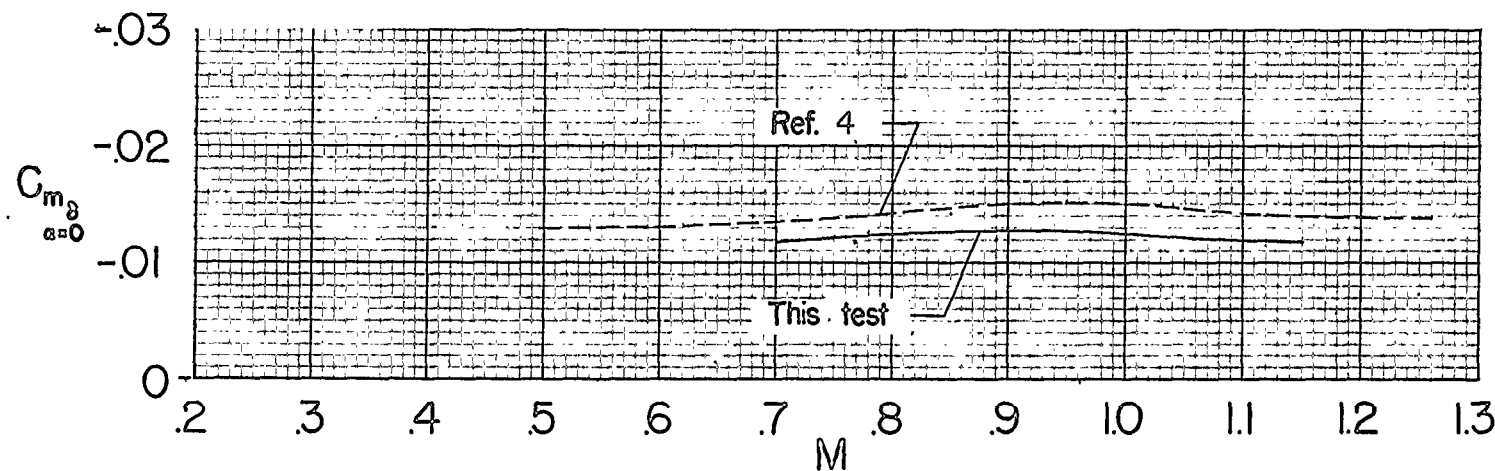


(c) Angle-of-attack ranges for various stability levels.

Figure 12.- Pitching moment summary.

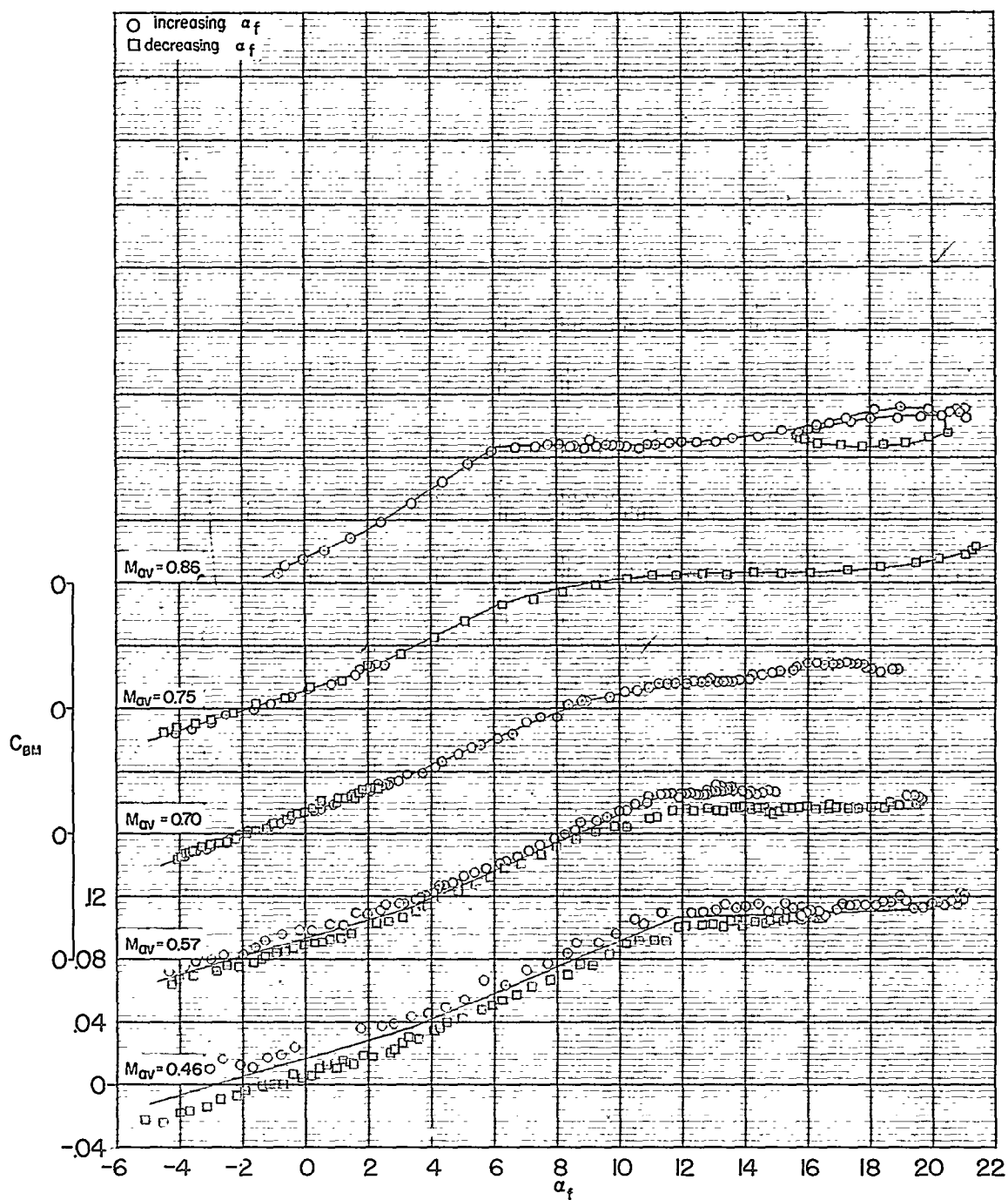


(d) Pitching-moment coefficient at zero angle of attack.



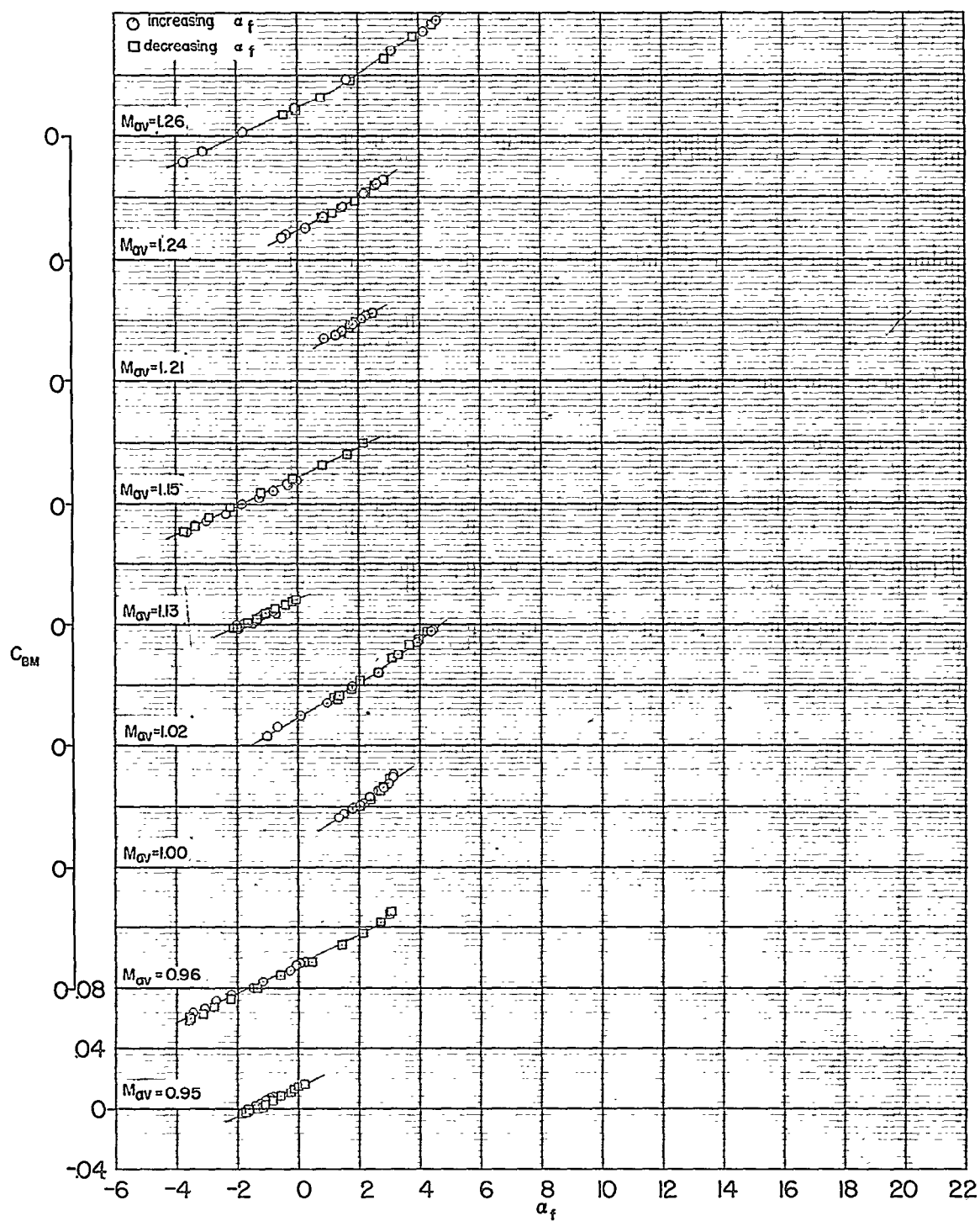
(e) Stabilizer pitching effectiveness.

Figure 12.- Concluded.



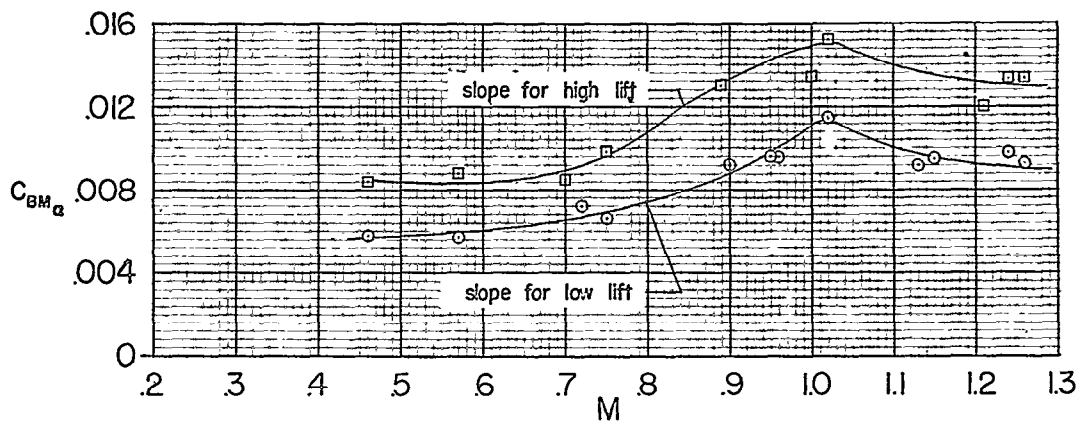
(a) Subsonic speeds.

Figure 13.- Basic wing bending-moment data.

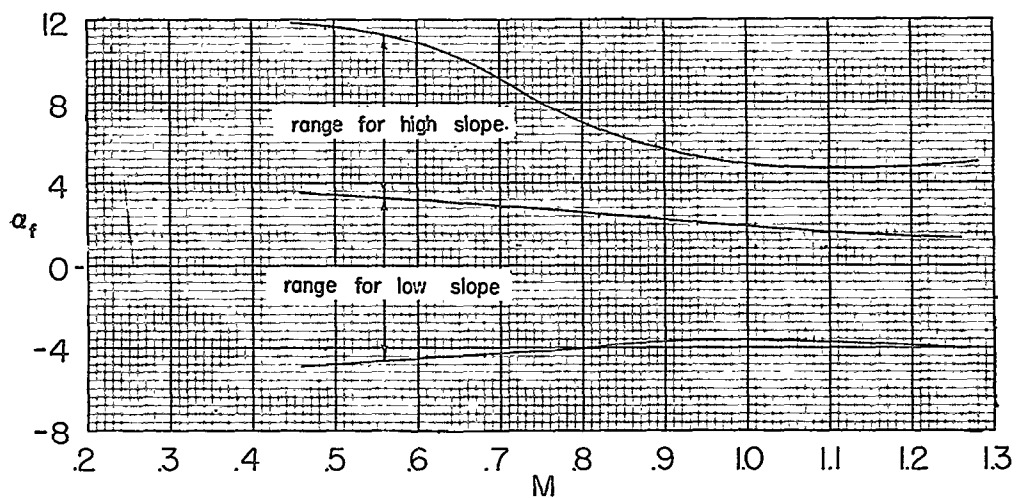


(b) Transonic speeds.

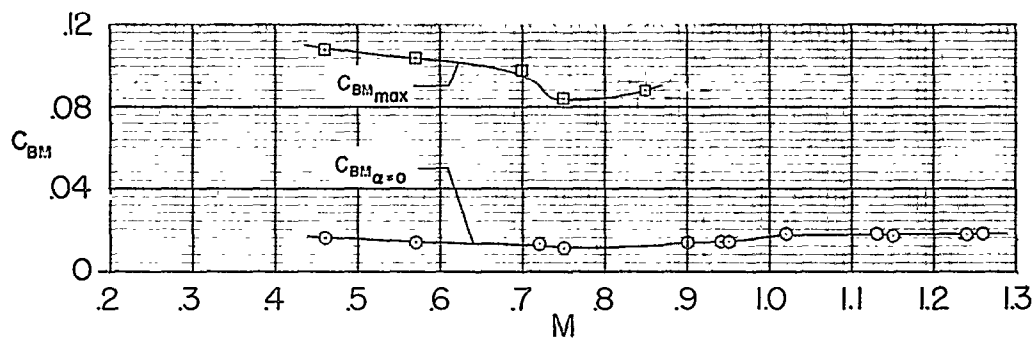
Figure 13.- Concluded.



(a) Bending-moment slope.



(b) Range of attack of angle for which slopes apply.



(c) Maximum bending-moment coefficient and bending-moment coefficient at zero angle of attack.

Figure 14.- Bending-moment summary.

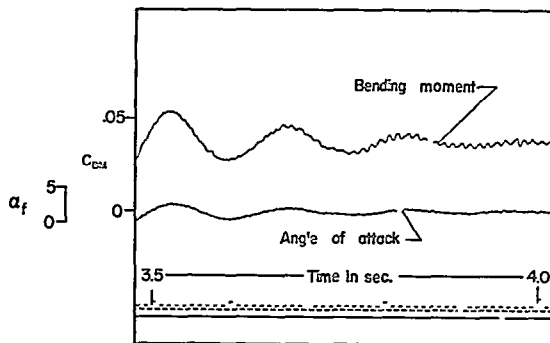
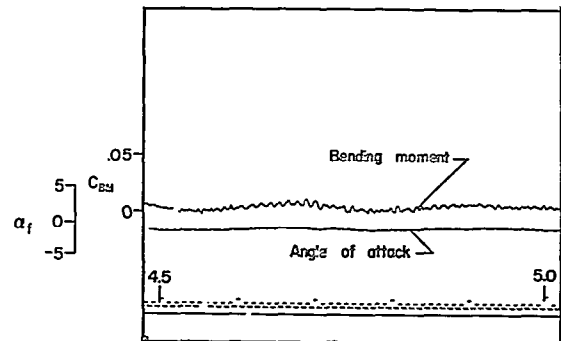
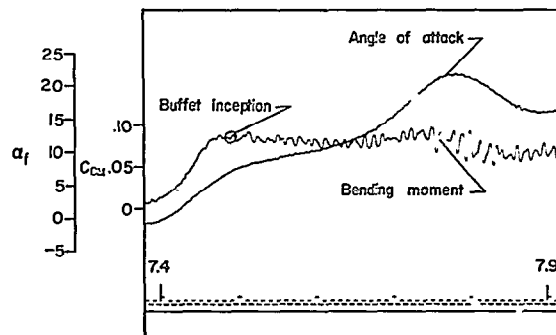
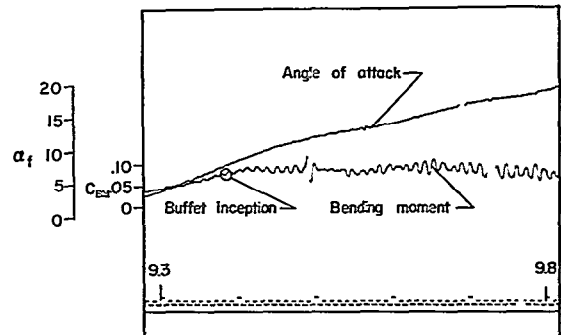
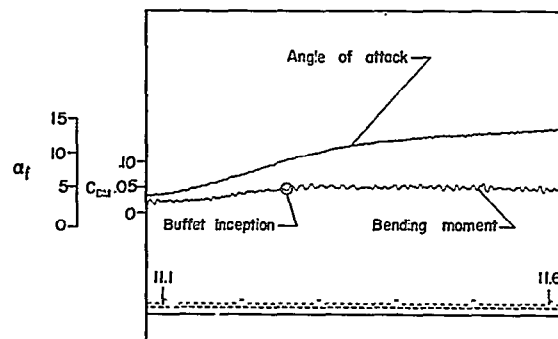
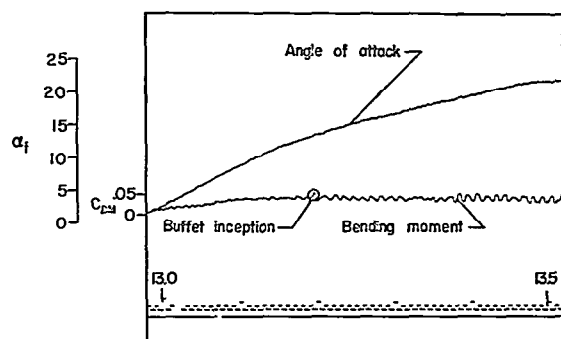
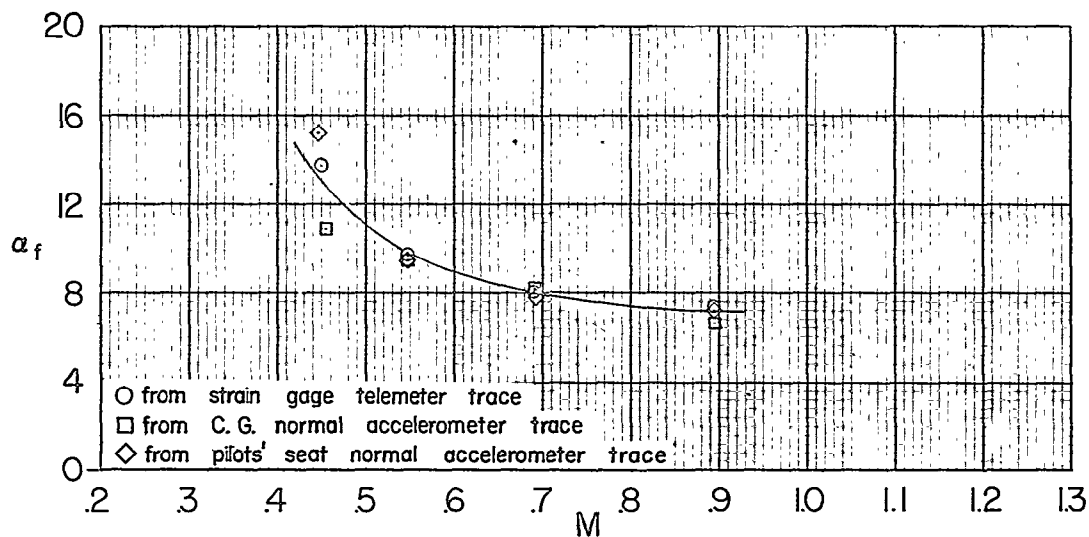
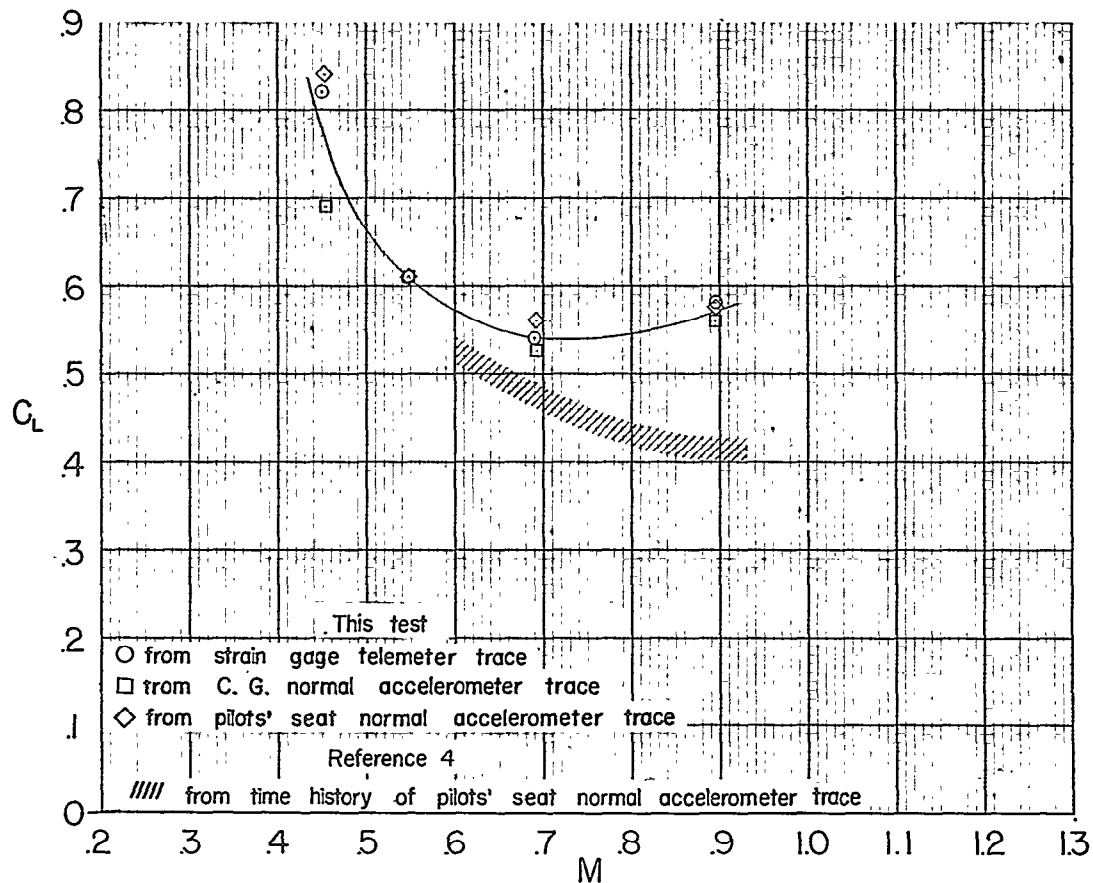
(a) $M = 1.23$ to 1.17 .(b) $M = 1.11$ to 1.06 .(c) $M = 0.90$ to 0.80 .(d) $M = 0.70$ to 0.63 .(e) $M = 0.56$ to 0.52 .(f) $M = 0.46$ to 0.43 .

Figure 15.- Portions of telemeter record showing buffet oscillations.



(a) Fuselage angle of attack at buffet inception.



(b) Lift coefficient at buffet inception.

Figure 16.- Buffet boundaries.

NASA Technical Library



3 1176 01438 9762

CONFIDENTIAL